SEARCH OF OPTIMAL CRUSTAL VELOCITIES USING WAVEFORM MODELLING OF LOCAL EARTHQUAKES

by

FEYZA NUR BEKLER

Submitted to
Boğaziçi University
Kandilli Observatory and Earthquake Research Institute
in partial fulfillment of
the requirements for the degree of
Master of Science
in
Geophysics

Boğaziçi University
2004

ACKNOWLEDGMENT

I could not have completed this thesis without the advice and support of many people both inside and outside Boğaziçi University. Prof. Mustafa Aktar provided direction for my thesis topic, as well as encouragement as a thesis supervisor. I would like to thank Prof. Mustafa Aktar.

I would like to thank Prof. Cemil Gürbüz, Prof Niyazi Türkelli who gave me a good start by helping me to understand data processing and rules of Seismology. In addition I would like to thank Assoc. Prof. Hayrullah Karabulut for sharing his know-how in order to use in my master thesis, I am grateful to him.

I would like to thank Assoc. Prof. Serdar Özalaybey for sharing source parameters of earthquakes and his valuable critic.

I would like to thank Dr. Tolga Bekler for his valuable critic and great deal of support.

I would like to thank Dr. Doğan Kalafat who helped me and shared his experiments about the magnitude calculation and digital broadband data processing. In addition, I remember about the useful discussions with Mehmet Yılmazer and Yavuz Güneş about the computer programming, I am grateful to them. I would like to thank Assoc. Prof. Gündüz Horasan and for developing which provided the database for this thesis.

Moreover, I deeply appreciate Prof. Balamir Üçer for his helps and supports in my thesis. Also, I am grateful to Ayşegül Köseoğlu and Ethem Görgün for sharing their experiences.

Of course, everyone dealing with Geophysics knows that research would come to stand-still without the work of the members of the support staff. Support staff at Kandilli Observatory National Earthquake and Department of Geophysics, TUBITAK Marmara Research Center, I would like to thank all of them. Furthermore, I would like to thank to the Administration staff of Kandilli Observatory and Earthquake Research Institute.

On the personnel side, I would like to acknowledge the support of my parents who taught me the value of a good education. I deeply appreciate my brother support and his fiance.

TABLE OF CONTENTS

LIST OF TABLES

LIST OF FIGURES

ABSTRACT

One of the concerns of geophysicist during the last decade is to reduce the damage of earthquakes. As a result, seismic hazard studies have become an integral part of long term planning and mitigation. One approach is to calculate peak ground acceleration (PGA) and use this scalar value in building design. However, this method has some disadvantages: it is very simple and it does not give spectral information related to the ground motion.
Generally, the effects of faulting type, source mechanism, rupture directivity, asperities are ignored during the calculation of the PGA values. The study in this thesis contributes to the simulation of the ground motion by constructing optimal crustal velocity models based on 1-D synthetic seismogram modeling. For this purpose, different crustal models were generated using the discrete wave-number technique (Bouchon, 1981) and they have been tested by searching the best-fit between observed and synthetic seismograms.

Waveforms from 5 earthquakes were analyzed in this study. The selected earthquakes have magnitudes larger than 3.5 and they are located along the main fault zone in the Sea of Marmara. The vertical, radial and transversal components were compared using the cross correlation coefficient between observed and synthetic seismograms. Crustal models having 5-layers with fixed depths were used to calculate the synthetics for each selected event. First, the optimum P-wave velocities were searched within predefined velocity limits for each layer. Once the optimum P velocities were obtained, then the S wave velocities have been searched. In general a moderate level of fitting is obtained even for the optimal crustal models. Although numerically the correlation values are quite low, the shapes of the waveforms are roughly close to each other, at least for some selected parts of the total waveform. The degree of fitting is particularly low in the part of the waveform where the 3-dimentional effects in the crust start to dominate, such as the P-arrivals in the transversal component. The performance also degrades with the level of the local noise, which is known to be not negligeable at ISKB station. The use of a clever search algorithm that uses a feedback mechanism to guide the search in a selective parameter space and accelerates the convergence towards the optimum (such as steepest descent, etc) will allow the scanning of wider range of parameter (eg estimating the layer depths in parallel to velocities, etc). This will certainely improve the results.

ÖZET

Son yıllarda jeofizikçilerin ana hedeflerinden biri de depremlerin zararlarını azaltmaya yönelik çalışmalar yapmak olmuştur. Bu nedenle, sismik risk çalışmalar uzun dönemler boyunca yapılan planlamalar ve depremlerin zararlarını hafifletmenin birer parçası olmuştur. Bu yönde yapılan yaklaşımlardan bir tanesi yer hareketini hesaplamak ve bulunan skalar değeri yapı planı hesaplarına uygulamaktır. Ancak bu metod bir takım dezavantajlar içermektedir. Oldukça basittir ve yer hareketi ile ilgili spektral bilgi vermez.

Genellikle fayın tipi, depremin odak mekanizması, kırılma yönü ve asperitelerin varlığı yer hareketi değerinin hesaplanmasında ihmal edilebilirler. Bu tezde yapılan çalışma, deprem kayıtlarına ve depremlerin faylanma parametrelerine dayandırılarak bulunan en optimal kabuk modelinin oluşturulması neticesinde ortaya çıkan yer hareketinin simulasyonuna katkı sağlamıştır. Bu amaçla ayrık dalga numarası tekniği (Bouchon, 1981) kullanılarak farklı kabuk modelleri oluşturulmuş ve bunlar simule edilen sismogramlar ve gözlemlenen sismogramlar arasındaki en yakın uyum tespit edilerek test edilmiştir.

Bu çalışmada 5 depremin dalga formları analiz edilmiştir. Seçilen depremlerin Mw > 3.5 ve lokasyonları Marmara Denizi içindeki fay düzlemi üzerindedir. Gözlemsel ve sentetik sismogramlar arasındaki kros-korelasyon katsayıları kullanılarak düşey, radyal ve transvers bileşenler karşılaştırılmıştır. 5 tabakalı kabuk modeli, seçilmiş olan depremlerin sentetik sismogramlar ile simule edilmesinde kullanılmıştır. Öncelikle P Dalgası hızları her bir tabaka için önceden belirlenmiş hız limitleri içinde taranmıştır. Genel olarak optimal kabuk modelleri için bile düşük seviyeli bir uyum sağlanmıştır. En uygun P dalga hızları elde edilmiş, daha sonra S dalgasına ait hızlar bulunmuştur. Gözlemsel ve sentetik dalgaların şekilleri birbirleri ile uyumlu gözükse bile korelasyon katsayıları biraz düşük bulunmuştur. Korelasyon değerleri rakamsal olarak oldukça düşük olmasına rağmen dalga formlarının biçimleri - en azından tüm dalga formu içinden seçilen parçalar için - kabaca birbirlerine çok yakındır. Uyumluluğun derecesi 3 boyutlu etkilerin kabukta etkin olmaya başladığı yerdeki dalga formu parçası içinde - örneğin P varışlarının transversel bileşende olduğu gibi - uyumluluk özellikle düşüktür. Kullanılan yöntemin performansı istasyondaki lokal gürültülerden dolayı, ki bu ISKB istasyonu için ihmal edilemeyecek kadar yüksektir, düşüş göstermiştir. Kabukla bağıntılı tüm parametreleri optimize etmeye yönelik bir arama algoritması kullanılması, sonuçların geliştirilmesine ve iyileştirilmesine yardımcı olacaktır.

CHAPTER I

I.1 Introduction

The Istanbul region has been repeatedly affected by damaging earthquakes during the historical period (Ambraseys and Finkel, 1991, 1995). Recently a destructive earthquake of magnitude 7.4 M_w that occurred in 17.8.1999 within a distance of 70 km also caused a significant damage. Nearly 6% of the total number of death (over 17000 in total) was located within the city of Istanbul. Frequent occurrence of historic destructive earthquakes clearly demonstrates the high seismic activity and the potential seismic hazard in the area. A major threat exists directed to both the population of over 10 million people that live in the metropolitan area of Istanbul, as well as to the industrial heartland of Turkey.

The minimization of the loss of life, property damage, and social and economic disruption due to earthquakes depends on reliable estimates of seismic hazard. The assessment of seismic hazard is first step in the evaluation of seismic risk obtained by combining the seismic hazard with local soil conditions and with vulnerability factors (type, value and age of buildings, infrastructures, population density etc). Seismic hazard is defined as the probable level of ground shaking associated with the recurrence of earthquake.

There are several conceptual models that are used for defining the seismic hazard at a given location. Broadly speaking there are two aspects to the problem of estimating the hazard. The first step is to describe as much realistically as possible the characteristics of the destructive ground shaking that is likely to occur in the area. The second step is to determine what would be the likelihood, in other word the probability of this destructive ground shake. The first step involves the definition of earthquake source, the distance, the wave propagation and attenuation factors, etc. The second step is concerned with occurrence characteristics this destructive earthquake model. The time-independent probabilistic (simple Poissonian) and time-dependent probabilistic (renewal) models are most preferred methods for studying the occurrence probability. In the Poisson process the probability of occurrence of next earthquake is independent of the time of occurrence of the previous one. In the time-dependent models, the probability of earthquake occurrence increases with elapsed time since the last major (or characteristic) earthquake on the fault that controls the regional earthquake hazard. The first model is more robust while the second one is more realistic and heavily depends on historical data, which is not often very reliable.

Estimates of expected ground motion at a given distance from an earthquake of a given magnitude are fundamental inputs to seismic hazard assessments. The determination of seismic design criteria for engineered structures depends on plausible, reproducible estimates of the expected ground motions from earthquakes during the expected lifetime of the structure. In practice the full description of the ground motion is seldom used, only peak values (eg. Peak Ground Acceleration, PGA) or occasionally the duration of the shake are the only parameters that determine the design criteria. The PGA estimates are usually obtained using empirical equations, called attenuation relationships, that express the peak value of the ground motion as a function of magnitude and distance (and occasionally site effects are also included). Attenuation relationships used in probabilistic earthquake hazard assessments predict ground motion parameters (PGA and SA) as a function of source parameters (magnitude and mechanism), propagation path and site effect (site class). Most attenuation models are based on statistical analyses of recorded ground motions which are updated as new strong ground motion data become available. Some attenuation models (e.g., Boore et *al.*, 1997; Campbell, 1997) distinguish between the faulting types ''normal'' and ''strike-slip'' because it is found that reverse and oblique mechanisms are associated with ground motions approximately 30-40 percent larger than strike-slip mechanisms.

The PGA value that is computed from attenuation curves does not give any information about the spectral properties of the ground motion. The important shortcoming of these regional attenuation relationships is the lack of a statistical representation of site classes.

It is clear that even though PGA has been in use for a long time by civil engineers a single scalar value such as the PGA is too restricted to give a full description of the true ground motion. On the other hand type of faulting, the full fault geometry, rupture directivity, existence and location of an asperity along the fault zone, strongly affect the ground motion but are not always considered while obtaining the attenuation curves. Recently, the synthetic seismogram modeling (waveform modeling) is used for a more realistic description of the ground shake. This is successfully used in seismic hazard studies especially in the low frequency range (<1Hz) in the context of large constructions, such as power plants, bridge, etc. A similar approach is now plausible for the city of Istanbul where a relatively detailed description of the fault geometry is now available (LePichon, et *al.* 2001). Preliminary efforts have been made along this line by Pulido et *al.* (2002), and by Aktar (2003).Aktar (2003) has made an effort to determine the effect of the location of the nucleation point, rupture direction, size and location of an asperity, upon the low frequency (<1Hz) part of the ground motion at an arbitrary point in Istanbul. For that purpose, he subdivided the fault area into several sub-faults of about 4x4 km, which were considered as individual point sources, and simply added the time delayed ground motion from each of them. Any complexity in rupture kinematics can be simulated by varying the nucleation point, the rupture velocity, which affect the time delay between consecutive cell, and the slip which determines the moment generated by each individual cell. In this approach, one of the main task is to determine the Green's function from each cell. It would be best to use real data to describe the contribution from each cell, however only a small portion of the cell contains aftershocks; therefore a theoretical Green's functions need to be computed for the remaining ones. The Discrete Wave number method of Bouchon (1981) is used to compute Green's function. Accordingly the flat-layered crustal model that is used for the generation of synthetic seismogram becomes one of the key factors to determine the performance of the approach.

Pulido et *al.* (2002) estimate near fault ground motion in broadband frequency range (0.1 to 10 Hz.) using a hybrid simulation technique that combines a deterministic wave propagation modeling for the low frequencies with a stochastic technique for the high frequencies. For the low frequency ground motion (0.1 to 1.0 Hz.) they subdivide the asperity into several sub-faults or point sources and simply add the time delayed ground motion from each of them by applying a constant rupture velocity. The seismogram from each point source is obtained numerically by the Discrete Wave number method of Bouchon (1981), which computes the wave propagation in flat-layered crustal velocity structure, for a given focal mechanism.

The high frequency ground motion (1 to 10 Hz) is calculated from the stochastic approach of Boore (1983). The idea of the stochastic method is to generate a random time series whose spectrum matches a specified spectrum of shear waves. The summation of the point sources is obtained by applying the empirical Green's function method proposed by Irikura (1986), which is very efficient for calculating the radiation of high frequency ground motion from finite faults. The ground motion from the point sources is calculated stochastically by using omega square model and applying a radiation pattern correction for an intermediate frequency range (Pulido, 2002). The main reason to use a stochastic Green's function in the Irikura technique is that in most of the cases there is no appropriate recording of an aftershock that can be used for the simulation. The calculation of a "stochastic Green's function" allows selecting the appropriate size of the "synthetic aftershock". It should be noted that, a "stochastic Green's function" has no information about the site effect, and therefore it can be only used to compute a bedrock ground motion, in contrast to the case of the recording from an actual aftershock.

In both approaches, it is clear that a reliable estimation of the Green's function that relates individual cell along the fault to arbitrary locations in Istanbul is needed. Accordingly, since the Greens functions are to be generated by using a flat-layered earth model, a realistic estimation of the crustal velocities becomes a crucial factor.

There are many methods that can be used for finding the best approximation for the flat-layered earth model. Some methods are reliable but do not have good resolution such as local earthquake arrivals (Gurbuz et *al,* 2000), Ergin et *al*, 1998). Other methods have resolution but have restricted coverage (Karabulut et *al,* 2003, Bekler 2002). In this thesis, a new method is applied which uses the earthquake occurrences along the possible rupture. These earthquakes are used to estimate the best crustal model that would simulate the actual recordings at a seismic station in Istanbul. This approach is motivated by the work of Ozalaybey et *al,* (2002), who point out that, a good fit between observed and calculated seismogram is possible by using a proper crustal model up to 1 Hz, together with a proper fault plane solution. These authors have solved the problem of finding the best fault plane solution, using the observed seismogram and a generic crustal model. Here, the same procedure is applied to solve the conjugate problem, which is to search for the best crustal model, knowing fault plate solution. For that reason, we have decided to use the data from the broadband station ISK and data from station TER but the same procedure can be applied to any station installed around Istanbul.

It must be clearly noted that the crustal models that are obtained in this approach are very approximate and should only be used to generate a more realistic ground motion when cell summation method is used. In other words, the models obtained are not adequate for making any interpretation in terms of the geological properties.

CHAPTER II

II.1 Tectonics

The active tectonics of northern Turkey is dominated by the right-lateral North Anatolian fault zone, running from Karliova in the east (41 °E) to Istanbul (29°E) in the west. Over much of this distance the fault zone is a clearly defined morphological feature that in some ways resembles a plate boundary in that it is narrow, localized and separates the rigid Black Sea and central Anatolia regions (e.g. McClusky et al., 2000). The zone has produced many large (Ms > 7) earthquakes with coseismic surface faulting and ruptured over most of its length this century in a sequence of large events between 1939 and 1999 (Ambraseys, 1970; Barka, 1996; Stein et al., 1997). Across most of Turkey, the North Anatolian fault is a relatively simple, narrow, right-lateral strike-slip fault zone; however it splits into several fault strands in the vicinity of the Sea of Marmara so that the deformation (surface faulting of the North Anatolian Fault) becomes distributed over an ~120 km broad zone (Taymaz et al., 1991; Smith et al., 1995; Okay et al., .1999, 2000; Parke et al., 1999; Aksu et al., 2000; Imren et al., 2001). East of about longitude 31° E the North Anatolian Fault system has a narrow and localized character, defined most obviously by the surface ruptures along almost its entire 1000 km length that were associated with a series of large earthquakes between 1939 and 1967 (Ketin, 1948; Ambraseys, 1970).

Right-lateral strike-slip faulting continues west of Izmit but becomes more distributed over several sub-parallel strands in the Sea of Marmara, NW Turkey and the northern Aegean (e.g. Barka & Kadinsky-Kade, 1988; Taymaz et al., 1991). The Sea of Marmara includes a series of tectonically active basins at the western end of the right-lateral North Anatolian Fault (NAF). It is 175 km long and 80 km wide with a broad shallow shelf to the south and a series of deep sub-basins to the north.

Seismic reflection surveys in the Sea of Marmara itself reveal many faults with large normal components (e.g. Smith et al., 1995; Okay et al., 1999; Parke et al., 2000), and earthquakes with normal-faulting mechanisms are seen around its margins (Ozalaybey et al., 2002, Orgulu, 2001). The Sea of Marmara was presumably formed by this component of crustal extension. Marmara still requires further investigations to better understand the complexity of active faulting associated with earthquakes.

Numerous damaging earthquakes have affected the Sea of Marmara region in historical time (Ambraseys & Finkel, 1991; Ambraseys & Jackson, 1998,2000; Ambraseys, 2001). Furthermore, Ambraseys (2001) argued that the seismicity of the western part of the

North Anatolian Fault zone is clearly different from that of many other parts of Balkans and southern Turkey. In recent years especially after the Gölcük earthquake of August 17, 1999, there is an enormous amount of scientific interest in the area. Many research projects have been conducted within the Sea of Marmara to better understand and to improve our knowledge of seismicity and seismotectonics settings. Imren et al. (2001) have summarized in great details the multi-channel seismic reflection method and discussed the proposed models, which appear to fit the earlier proposition of Le Pichon et al. (1999).

II.2 The Sea of Marmara Fault System

To the east of the Sea of Marmara, the North Anatolian fault (NAF) has a single trace where deformation has been limited to a narrow zone over several million years (Hubert-Ferrari *et al.,* 2002a). At the eastern end of the Sea of Marmara, the fault splits into two systems (even possibly more), the Northern segment, North Anatolian Fault (NAF) and the Southern segment, North Anatolian Fault (SNAF). The NNAF passes through the Marmara Sea to the Dardanelles while the SNAP passes on land to the South. In recent years, the NNAF was substantially more active than the SNAP (Figure 2.1). The strike-slip deformation on both branches then continues into the Aegean where it interacts with extension that has been active for the last 15 Myr. The NAF appears to have evolved by propagation from east to west (Armijo *et al.,* 1996; Hubert-Ferrari *et al.,* 2002a). According to Armijo *et al., (*1999), it initiated in Eastern Turkey between 15 and 10 Ma as a result of the collision of Arabia and Eurasia and crossed the western Marmara Sea at 5 Ma. Further propagation has resulted in the reactivation of the Gulf of Corinth at 1 Ma (Armijo *et al.,* 1996).

Within this context, Armijo *et al., (*2002) argued that the Marmara Basin has evolved over the last 5 Ma mainly as a result of strike-slip motion and it can be identified kinematically as a pull-apart (in the offset between the NAF and the NNAF) with some minor complexities. These geological reconstructions suggest that, while Aegean extension may play some initial role in creating the Sea of Marmara structures, overall extension perpendicular to the overall trend of the NAF is not required to reconstruct the geology.

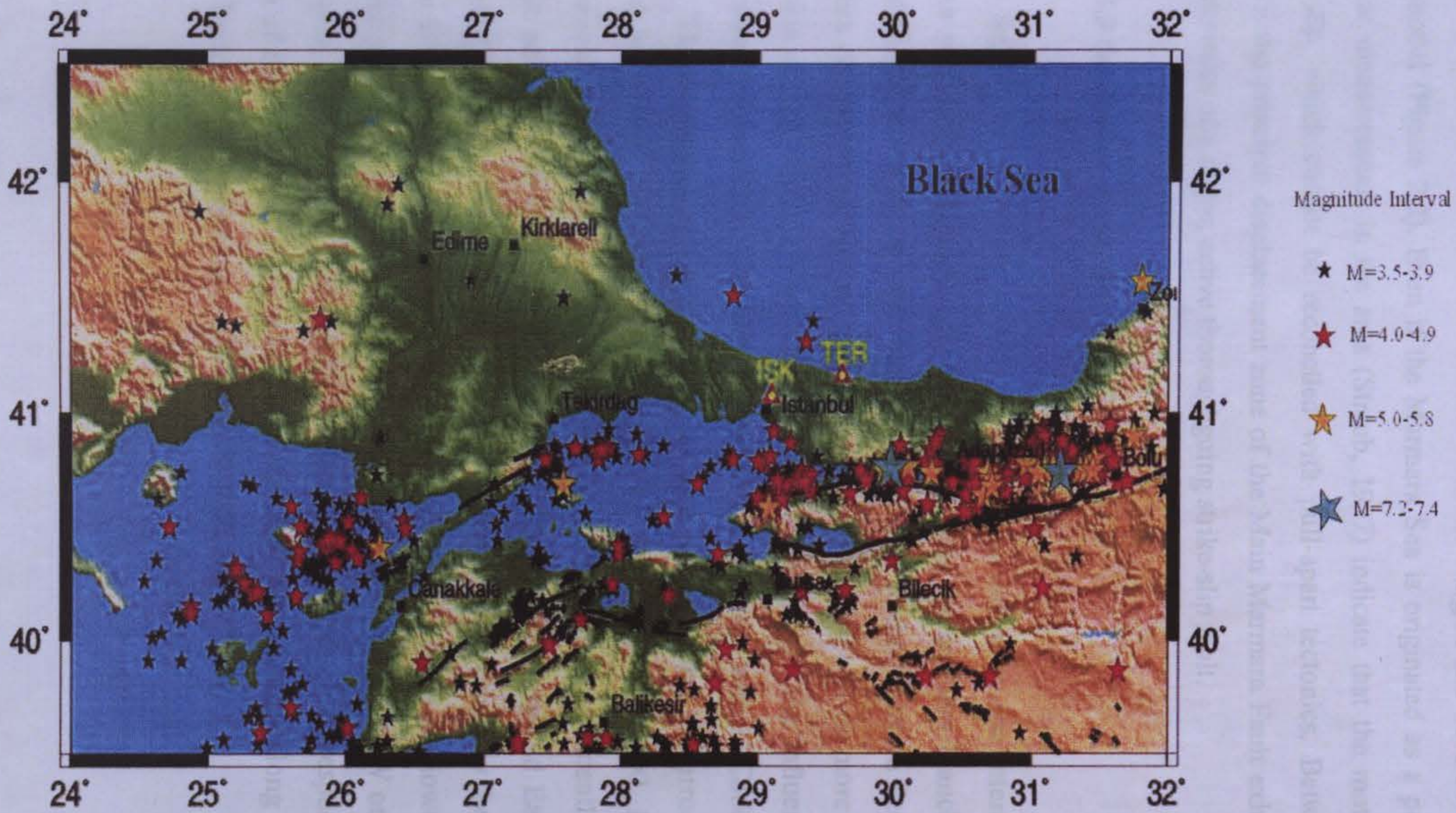

Figure 2.1 Seismicity of the region. Seismicity is taken from KOERI catalogue for M >3.5 earthquakes that occurred during the 1990-2004.

Pichon et al., (2001) have a different view, they argue that there is a continuous fault across the Sea of Marmara that does not coincide with the margins and does not fit the simple pull-apart. model (Figure 2.2). Even if the Marmara Sea is originated as a pull apart, the dense geodetic measurements in the area (Straub, 1997) indicate that the motion there is purely strike-slip, which cannot be reconciled with pull-apart tectonics. Between 28^0 48'E and $27^0$24'E the principal displacement zone of the Main Marmara Fault exhibits all the typical characteristics of a major, active thoroughgoing strike-slip fault.

II.3 Seismicity of the Marmara Sea

Seismicity of Turkey is well known and governed by the interaction of Eurasian, Arabian and African. Seismic activity is linear along the northern branch of NAF, but it is more diffused on the Bursa/İznik branches, southeast of the Marmara Sea. Seismicity in the Marmara region is a result of tectonic movements along two or more possible westward extension of the NAFZ beyond the Mudurnu valley where the influence of the Aegean extensional tectonic regime has been recognized (Barka and Cadinski-Cade, 1988).

The seismicity and tectonics of the Marmara Sea and its surroundings have been studied by several authors (Ucer et al., 1997; Gurbuz et al., 2000, Ergin et al., 1998, Orgulu and Aktar, 2001, Ozalaybey et al., 2002), but it is only recently that a permanent seismic network has been installed by the Kandilli Observatory and Earthquake Research Institute (KOERI) and TUBITAK in order to monitor more accurately the earthquakes of the region. Depth distribution of the seismicity in the whole area is shallower than 20 km. The northern part of the Marmara Sea, at latitude of 40^o0.8N, shows an EW oriented alignment of epicenters, from Izmit to Gaziköy (NW Marmara Sea), which corresponds to the northern branch of the NAF. The southern branch of the NAF, which passes along the southern border of the İznik Lake, is mostly active between 28^o0.6E and 29^o0.4N.

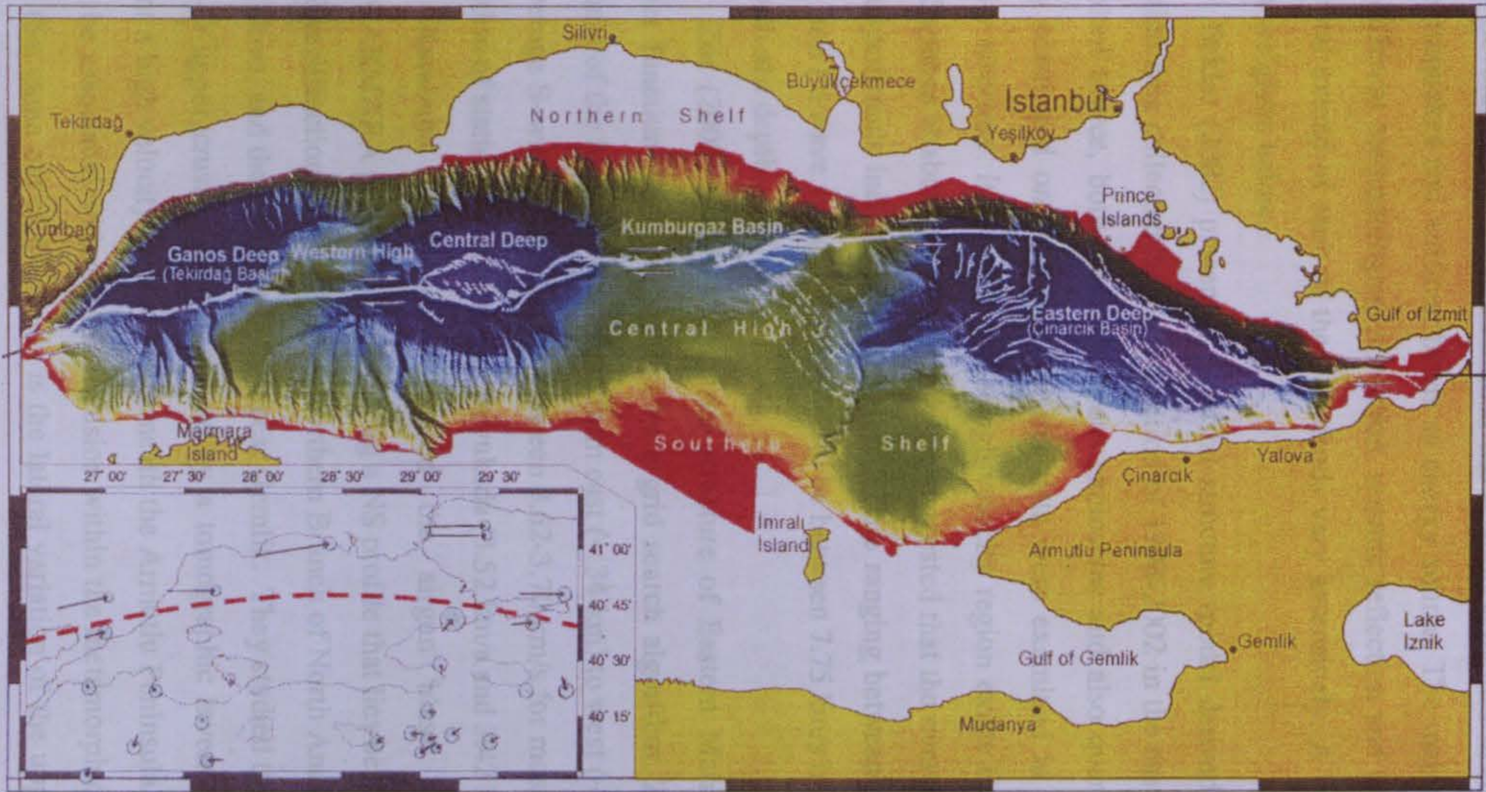

Figure 2.2 Bathymetric map of the Marmara trough with main active structure. Main active faults are shown by tick lines (X. Le Pichon et al., 2001)

II.4 Previous Studies of Eastern Part of Marmara Region

Several authors have examined the seismic velocities in the Marmara Region, using both earthquakes and artificial blasts as energy source. The major approaches are based on three different methodologies: refraction, seismic reflection and tomography. The depth and horizontal extend of each of these methods vary extensively. A brief overview of some the results are given below.

Bekler (2002) presented a crustal structure model derived from analysis of seismic refraction data collected during the period of 1998-2002 in the eastern Marmara region. As a controlled source, both special purpose explosives and also quarry blasts were used. Two quarry blasts and one controlled source data were examined in order to obtain a reliable velocity structure. It is noted that a high velocity region exists between the Lake Iznik and Lake Sapanca at about 6 –7 km depth. He suggested that the overall pictures of the all quarry blast experiments indicate that Pg velocities are ranging between 5.4-5.7 km/s for the upper crust, and Pn wave velocities are found to be between 7.75 km/s in the south and 7.95 km/s in the north at a depth of 32-35 km.

Zor (2002) studied the crustal structure of Eastern Marmara region. He used the receiver function modeling method by a grid search algorithm. Zor (2002) determined the thickness of the Marmara Sea crust, from east (~ 34 km) to west (~ 28-32 km). He found that the average S–wave velocities are between 3.62-3.70 km/s for most of the study area with the exception of stations Bozburun and Buyukada (3.52 km/s and 3.42 km/s).

Karabulut et al., (2003) used the airgun blasts that were made during SEISMARMARA project recorded along a NS profile that lies between Uludag Mountain and Şile. The refraction line crosses the Northern Branch of North Anatolian Fault between Gebze and Yalova, and the southern branch near Gemlik. They studied the first arrivals and revealed the 2-D upper crust velocity structure by a tomographic inversion approach. Their results present a high velocity anomaly underneath the Armutlu Peninsula. They pointed out that this might be associated with granitic intrusion within the metamorphic body. Another interesting result that came out of this study is the lateral variation of the upper crsutal velocities along the north-south profile. In fact, the velocities which coincide with the intersection of the profile with the branches of the North Anatolian Fault have velocities considerebly lower than the surrounding bodies.These low velocity bands corresponds also the sections where most of the aftershocks are located after the 1999 Izmit Earthquake.

Imren et al. ,(2001) studied a total of 2200 km of multi-channel seismic reflection data collected during various campaigns. The energy source was an air gun. They present the northern Sea of Marmara Basins as been cut by a single strike-slip fault system, that they call the Marmara Fault. It links the İzmit Fault (striking 270^0)of the northern branch of the North Anatolian Fault, in the east, to the Ganos Fault (striking 245^0) to the west. East of Ganos, the fault abruptly changes to a 265° direction than it continues for about 80 km. Then it turns southeastward along the northern slope of the Çınarcık Basin for over 65 km in a 280° direction. This eastern part of the fault has two parallel branches, 2-5 km apart. The motion along the northern branch is transferred westward through an E-W shortening zone that occupies the northern half of the Çınarcik Basin and of the adjacent eastern Central High, and extends over a 30 km width. It is probably no coincidence that this shortening zone appears where the northern slope changes from its 295° direction to a 270° one. The two branches are parallel and very close, according to Imren et al., (2001) and they correspond to the same active fault at depth, at least in the eastern Çınarcık Basin. Thus the active Marmara Fault system is essentially a continuous dextral strike-slip fault between the İzmit Fault to the east and the Ganos Fault to the west. They further argue that the present tectonic structure is not a pull-apart structure. Actually, they did not found any evidence for significant active normal faulting in the northern Sea of Marmara Basins. They also noted that a microseismicity study of the northern basin has shown that fault plane solutions are either strike-slip or compressional and that the stress tensor is compatible with pure strike-slip on the approximately E-W fault system.

Gurbuz et al. (2000) studied the seismotectonics of the Marmara region using observation from a microseismic experiment. A total of 137 microearthquakes were located and 23 of those were selected to obtain the focal mechanism solutions. According to Gurbuz et al., (2000) the epicentral distribution indicates that the activity is very linear along the northern branch of the NAF, but it is more diffused on the Bursa and Iznik branches, southeast of the Marmara Sea. The stress tensor obtained from the focal mechanisms of the micro-earthquakes is compared to the one inverted from teleseismic data. It shows that there is an overall domination of the right lateral regime in addition to an extension which becomes more important as we go to the west.

Ozalaybey et al., (2002) found the dominance of the mainly strike slip motion character of 1999 Izmit earthquake sequence. They located four events off the Princes Island indicate similar mechanism characterized by right-lateral strike-slip motion parallel to the strike of the Northern Boundary Fault. They also indicate that the coexistence of strike slip and extensional seismotectonic features in the Sea of Marmara highlight the importance of strain partitioning amongst shallow transtentional structures accommodating north-south extension and deeper structures associated with the NAF accommodating east-west right-lateral shear. They also reported final velocity model in Table 2.1. These results are important to determine main fault geometry and its strain accumulation for the NAF within the Sea of Marmara because it is highly critical for any realistic seismic assessment for the city of Istanbul and other metropolitan areas of the Marmara region.

Depth(km)	Vp(km/sec)
0.0	2.9
1.0	5.7
6.0	6.1
20.0	6.8
33.0	8.05

Table 2.1 Marmara Region Velocity Model proposed by Ozalaybey et al. (2002)

CHAPTER III

III.1 Basic Approach

We model the ray path between the epicenter and the station by a Green's Function. The Green's function translates the simplest displacement at a source point (impulse both in time and space domain) described by its moment tensor components, away to a specific point, which is the station. The major aim is to find the Greens functions, which best fit with the observed data. We have simulated the waveforms of five earthquakes of the Marmara region with magnitudes greater than 3.5 to determine an optimum crustal structure. The waveform data used in the study were obtained from Bogazici University, Kandilli Observatory and Earthquake Research Institute and TUBITAK Marmara Research Center database. The waveforms are recorded at ISK station (Istanbul-Kandilli) and at TER station (Şile-TUBITAK) where 3-component broadband seismometers are used. The fault plane solutions were obtained from previous studies that have used polarity of P-arrivals. Using the discrete wave number technique (Bouchon, 1981), different layered crustal models have been tested for the simulation of the waveforms, and the best crustal model was determined by finding the best fit between the observed and the synthetic waveforms.

The total procedure is outlined in a flow diagram in Figure 3.1. As seen clearly from the figure, the searches for an optimal crustal model is a looping procedure that changes the crustal model based on the one that was used in the previous step, synthesize a new seismogram with the newly obtained crustal model and compare it with the observed data.

First the observed seismogram is prepared for the search process. In ISK Broadband station, the input data was available at GCF format. The GCF format was first converted to SAC format by using Scream (3.1) program (Guralp, 2002). The mean, the linear trend of the data are removed for signal correction. We also remove the instrument response of each record using the SAC routines and the pole-zero information. The observed data are then converted into radial and transversal components.

Next the synthetic seismogram is obtained. The synthetic seismograms are computed for 3 geographical components (East-West, North-South and Vertical) using the discrete wave number technique (Bouchon, 1981). The fault plane solutions were obtained from Ozalaybey

(2003) and Orgulu (2001). All the earthquke sources are rigth-lateral strike-slip fault with a focal depth of about 10 km. In searching for the best fit, the crustal models were modified sequentially at each step by incrementing P-velocity at each layer. The synthetic data is then converted into radial and transversal components. The correlation coefficient between all three components of the observed and synthetic data is evaluated for the comparison. The iteration is repeated until a full test of all possible models is completed for P-waves. At each step the maximum value of the correlation coefficient is found and is noted together with the corresponding crustal data. Once the search is completed for P-velocities, all the correlation values obtained are sorted and the model that provides the highest correlation coefficients is chosen as the optimal one. After the search for the optimal P-wave structure, the same search procedure is repeated for S-velocities. The final optimal crustal model is therefore the one that gives the highest correlation for both the P- and the S-velocities.

Occasionally, arrival times for a given crustal model were also tested in such a way that the computed arrivals do not deviate too much from the observed ones.

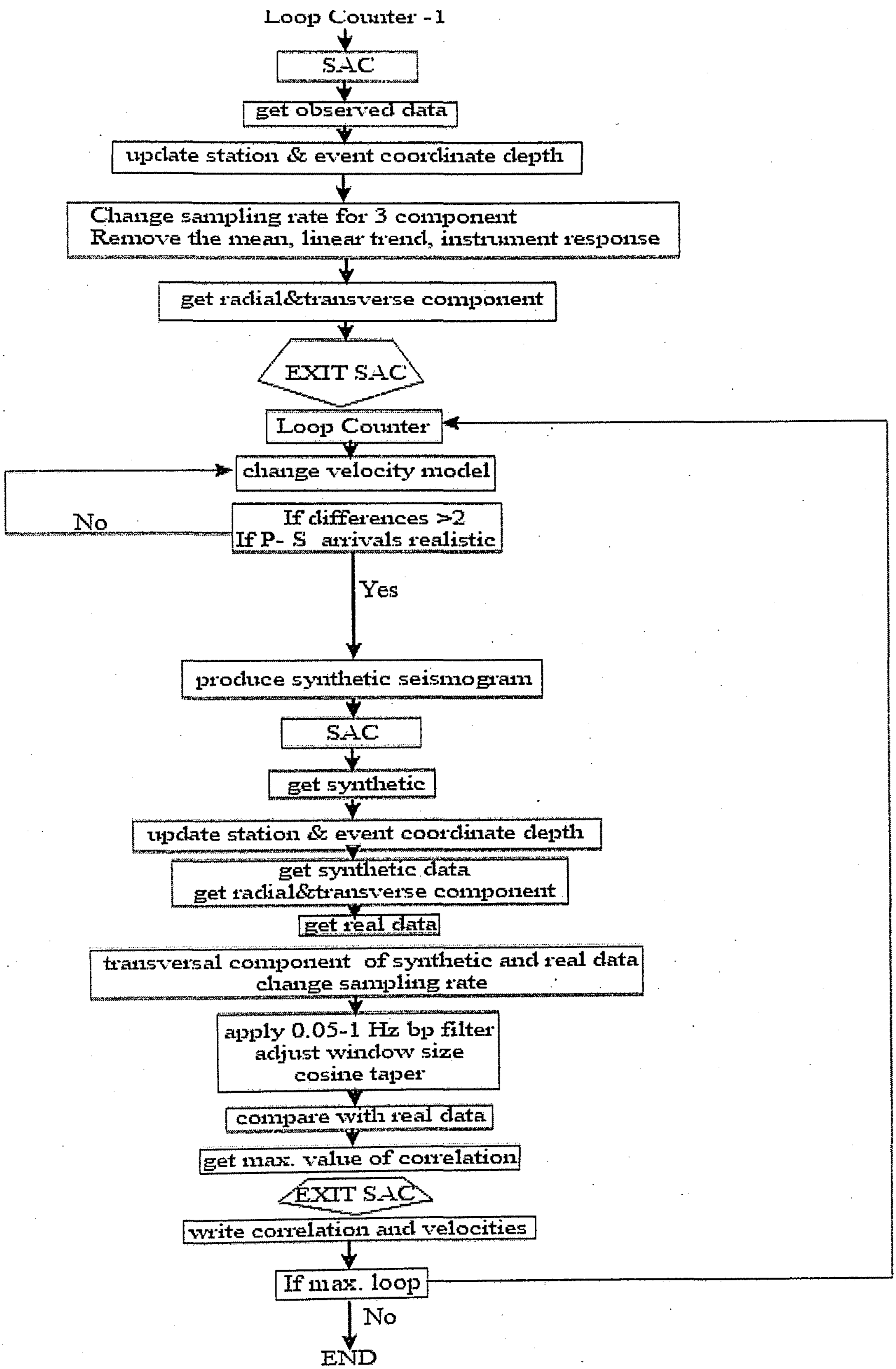

Figure 3.1 Flow chart of data processing.

III.2 Crustal Structures for testing

In present study, we are representing the crustal velocity structure by constructing a 5-layered model. The thickness of each layer is held fixed (2, 6, 14, 13 km and half medium below Moho) while the P- and S-values are changed sequentially at each step. The densities at each layer is calculated from the P-wave velocity using an empirical relation:

$$\text{density} = 0.32\ Vp + 0.77 (\text{numerically}) \text{ (Berteussen, 1977)} \qquad (1)$$

The Q values are held fixed for each individual layer. We have noted that modifying the density or the Q values within a realistic range do not effect the waveforms significantly within the frequency range that we are interested. The P-velocities for each layer are allowed to change by 0.1 km/sec in a predetermined range. The span of the search range for each layer together with the values, which are held fixed, are tabulated in Table 3.1.

Layer	Depth (km)	P Velocity Range (km/s)	S Velocity Range (km/s)	Density(gr/cm^3)	P Quality	S Quality
1	2	1.5-4.6	1-1-2.7	1.25-2.24	300	150
2	8	5.5-6.0	2.8-3.3	2.53-2.69	300	150
3	22	6.1-6.8	3.4-3.8	2.72-2.96	300	150
4	35	6.9-7.4	3.9-4.2	2.97-3.13	300	150
5	0	7.5-8.0	4.3-4.7	3.17-3.33	300	150

Table 3.1 Contents of 'dap.dat' input file.

In some situations, the scan range was reduced based on experience that was gained from the previous search of another earthquake. The generation of the updated crustal model is done using a FORTRAN program that reads the model used in the previous step, increment the velocity by 0.1 km/sec starting from the shallowest layer. Once the search limit for a given layer is attained, the program, increment the velocity of the next layer by 0.1 km/sec and repeats the process until a full search of all possible combinations of velocity values are tested.

III.3 Discrete Wave number Method

The evaluation of Green's functions for elastic media is an important problem in seismology. The discrete wavenumber method, introduced by Bouchon and Aki(1977), provides a way to accurately calculate the complete Green's functions for many problems with a minimum amount of mathematics. The discrete wavenumber (DWN) method introduces a spatial periodicity of sources to discretize the radiated wave field, and relies on the Fourier transform in the complex frequency domain to calculate the Green's functions. The steady-state radiation from a line source in an infinite homogeneous medium can be represented as a cylindrical wave or equivalently, as a continuous superposition of homogeneous and inhomogeneous plane waves.Therefore, denoting by x and z the horizontal and vertical axes in the plane normal to the line source, any observable such as displecement or stress can be written in the form,

$$F(x,z;\omega) = e^{i\omega t} \int_{-\infty}^{\infty} f(k,z) e^{-ikx} \, dk \qquad (1)$$

where w is the frequency and k is called the horizontal wave number.

When the medium is finite or vertically heterogeneous, the integral kernel has poles and singularities, and the integration over the horizontal wave number becomes mathematically and numerically complicated. One simple way around these difficulties is to replace the single-source problem, whose solution is expressed by (1), by a multiple-source problem where sources are periodically distributed along the *x-axis*. Then, equation (1) is replaced by:

$$G(x,z;\omega) = \int_{-\infty}^{\infty} f(k,z)e^{-ikx} \sum_{m=-\infty}^{\infty} e^{ikmL}\, dk \tag{2}$$

where L is the periodicity source interval and the e^{ixt} is the time dependence. Equation (2) then reduces to:

$$G(x,z;\omega) = \frac{2\pi}{L} \sum_{n=-\infty}^{\infty} f(k_n,z)e^{-ik_n x} \tag{3}$$

with

$$k_n = \frac{2\pi}{L} n$$

if the series converges, it can be approximated by the finite sum equation

$$G(x,z;\omega) = \frac{2\pi}{L} \sum_{n=-N}^{N} f(k_n,z)e^{-ik_n x} \,. \tag{4}$$

the problem from one of a single source, to one involving an infinite number of periodic sources. The DWN method calculates equation (4), that is *G(x,z;w),* instead of evaluating equation (1).

The second stage of the method is to retrieve the single-source solution from the multiple-source problem that we have solved in the frequency domain. This would be straightforward if we could calculate the continuous Fourier transform of *G,* as we could then isolate the single source solution in the time domain, provided that we have chosen an appropriate value for *L*. In practice, however, we can only calculate *G* for a certain number of frequencies and use the discrete Fourier transform to obtain the time domain solution. Thus, on one hand we deal with a signal which has an infinite time response (because of the infinite set of sources), while on the other hand, we use the discrete Fourier transform, which yields a signal of finite duration $T=2\prod/\Delta w$ where Δw is the angular frequency sampling used in calculating *G*. This can indeed be accomplished by performing the Fourier transform in the complex frequency domain:

$$g(x,z;t) = \int_{-\infty+i\omega_I}^{\infty+i\omega_I} G(x,z;\omega)e^{i\omega t}\,d\omega \tag{5}$$

where w_I denotes the constant imaginary part of the frequency and is chosen such that

$$e^{\omega_I T} << 1.$$

the time-domain single-source solution *f(x,z;t)* is obtained from the frequency-domain multiple-source calculation *G(x,z;w)* by

$$\mathrm{f(x,z;t)} = e^{-\omega_I T} \int_{-\infty}^{\infty} G(x,z;\omega)e^{i\omega_R t}d\omega_R \tag{6}$$

where the integral is computed by using the FFT.

$$\omega 1 = -\frac{\pi}{T}, -\frac{2\pi}{T} \tag{7}$$

The choice of $\omega 1$ may also be justified by the fact that the frequency spectrum *G(ω)* is not discrete, as would be the case with real frequencies, but is continuous with a bandwidth proportional to $\omega\ 1$ (Larner, 1970). The calculated signals may also be considered as resulting from a nearly continuous sampling of the frequency domain. Firstly, an input file was constructed to compute a synthetic seismogram. This file includes the source parameters, the crustal parameters and the waveform parameters. The crustal parameters are number of layers and their thickness values, P and S velocity, density, Q values for each layer. We describe the source by its strike, dip, rake, azimuth, rise time, amplitude of slip, length and the width of the fault. The waveform parameters include the distance to receiver, time window length, and number of points. Each seismograms is computed up of 512 points and we used length of the time window 64 for the synthetic seismograms.

III.4 Rotation of Seismograms

In many applications involving directional quantities it is more convenient to convert quantities from one coordinate system to another. In this application we rotate the signals from geographic coordinates (NS, EW, vertical) to the radial – tangential system which effectively align the seismometers with the direction of ray path. The problem is to use the observed north and east components of ground motion to compute the radial and tangential components. Seismograms are generally recorded with vertical (not shown), north and east components. Analysis is often easier when these observations are rotated into the radial-tangential coordinates where P – SV – Rayleigh waves are separated from SH – Love waves. The radial is the direction along the great circle connecting the epicenter to seismometer, and it is positive in a direction away from the source. We can perform the rotation using a matrix multiplication of a vector consisting of the north and east components with rotation matrix given by

$$A = \begin{bmatrix} \cos\phi & \sin\phi \\ -\sin\phi & \cos\phi \end{bmatrix} \tag{8}$$

Then we have

$$\begin{bmatrix} R \\ T \end{bmatrix} = A.\begin{bmatrix} N \\ E \end{bmatrix} \tag{9}$$

By using the back-azimuth, North-South and East-West components can be rotated into the radial and tangential components. The back-azimuth is defined as the angle measured between the vector pointing from the station to the source and the vector pointing from the station to the north (Sherbaum and Johnson, 1992). The reason why we want to obtain ray based radial and tangential components is that P–to–SV mode conversions are radially polarized and should be present primarily on the radial component.

In practice we used a built-in function (command: *rotate*) from SAC routines to perform the component rotations. When the coordinates of the station location and event hypocenter are inserted, and when the three geographical components (NS, EW, Vertical) are marked individually into the waveform header, the rotation is done by a single command.

III.5 Bandwidth Selection

It is clear that the velocity analysis has a lower and higher frequency limits, which are imposed by the maximum dimension of the crustal path that we are studying (about 120 km) by the vertical resolution that we are interested (about 2-3 km) and the bandwidth of the seismometers. In general, modeling of the ground motion for studying the hazard in cities, is done in two different frequency band. The generation of the synthetic seismogram using deterministic forward procedures are limited to the low frequency end, and do not extend beyond 1 Hz. The higher frequency band, i.e. for frequency > 1Hz, we never have high-resolution velocity data in order to produce realistic synthetics. In that high frequency range, random stochastic processes are usually generated that fit the available real data in terms of power spectrum. In this thesis the high frequency limit is therefore fixed to 1Hz, as often done in practice. The low frequency is limited to 0.05 Hz, because considering the size of the events and distances that are used for simulation ($3.0<M<4.5$), we do not expect to have signal energy in frequencies lower than this limit. Despite this general approach, the frequency range needed some minar adjustements around a small margin in some cases in order to obtain a better fit.

III.6 Search for a best fitting waveform: correlation

The correlation coefficient gives a measure of the similarity of the shape of the waveform of two signals. We measure the correlation coefficient to find the similarity between the observed and the synthetic seismograms, in the way to determine an optimum velocity structure. Numerically, the correlation discrete function is obtained by using the following expression

$$r(l)=\frac{\sum_i (x_i)(y_{i+l})}{\sqrt{\sum_i (x_i)^2}\sqrt{\sum_i (y_i)^2}} \qquad (10)$$

where x_i symbolizes the observed seismogram y_i is symbolizes the synthetic seismogram, and l the time shift where the correlation is calculated. In order to normalize, we divide the cross-correlation values with the square root of the product of the energies of each signal.

In reality since we want to make the comparison for a small range possible values of delay between the two signals, we first calculate the correlation function for a given range of l and then get the peak value, which describes the best fitting position. A FORTRAN program is written for that purpose. It takes the cross-correlation of the radial, vertical and transversal separately, within a time window of +/- 1.5 sec about the zero time shift (i.e. $-12<l<12$, for a sampling period of T=0.125s). A separate cross-correlation function is obtained for each component and the point where all three functions commonly reach their highest value is selected as the optimum cross-correlation delay.

The best crustal velocity model is assumed to be the one, which gives the maximum cross-correlation coefficient at all three components. Once the search is completed for P-velocities, all the correlation values obtained are sorted and the model that provides the highest correlation coefficient is chosen as the optimal one. After the search for the optimal P-wave structure, the same search procedure is repeated for S-velocities. A minor off-line re-adjustment of both the velocity values and the comparison frequency range was often necessary in order to reach the final optimal crustal model.

To calculate the correlation coefficient, we have used a time window, which includes whole P wave and the first few seconds of the S wave. This way we exclude any complication that may come spurious peaks from S-wave coda. These best obtained coefficients range from 0.1 to 0.5 for all components. It is clear that these values are relatively low as also noticed from the waveforms themselves. Correlation values reaching level of 0.9 were obtained for individual components but when a model that satisfies all three components is required, the performance degrades drastically. Needless to say that a more improved search algorithm will perform better.

For the best model the correlation coefficients between the observed and synthetic waveforms for five earthquakes are shown in Table 3.2.

Earthquake	Vertical component correlation coefficient	Radial component correlation coefficient	Transversal component correlation coefficient
020323-0236(ISK)	0.27	0.39	0.21
990817-0554(ISK)	0.31	0.21	0.31
010324-1307(ISK)	0.21	0.34	0.10
020228-0837(ISK)	0.27	0.31	0.32
020228-0837(TER)	0.29	0.51	0.45

Table 3.2 The list of correlation coefficient.

III.7 What were the main factors for selecting earthquake?

The data used in this study were obtained from the Bogazici University, Kandilli Observatory and Earthquake Research Institute and TUBITAK Marmara Research Center database. The recording systems are broadband high dynamic range instruments. Waveform from five different earthquakes is investigated. The locations of the earthquake epicenters are given in Table 3.4 and mapped in figure 3.2. Ideally; the method requires the simulation of all earthquakes along the rupture path and at all various depths. But this is nearly impossible because there are not enough earthquakes that have occurred along the total length of the

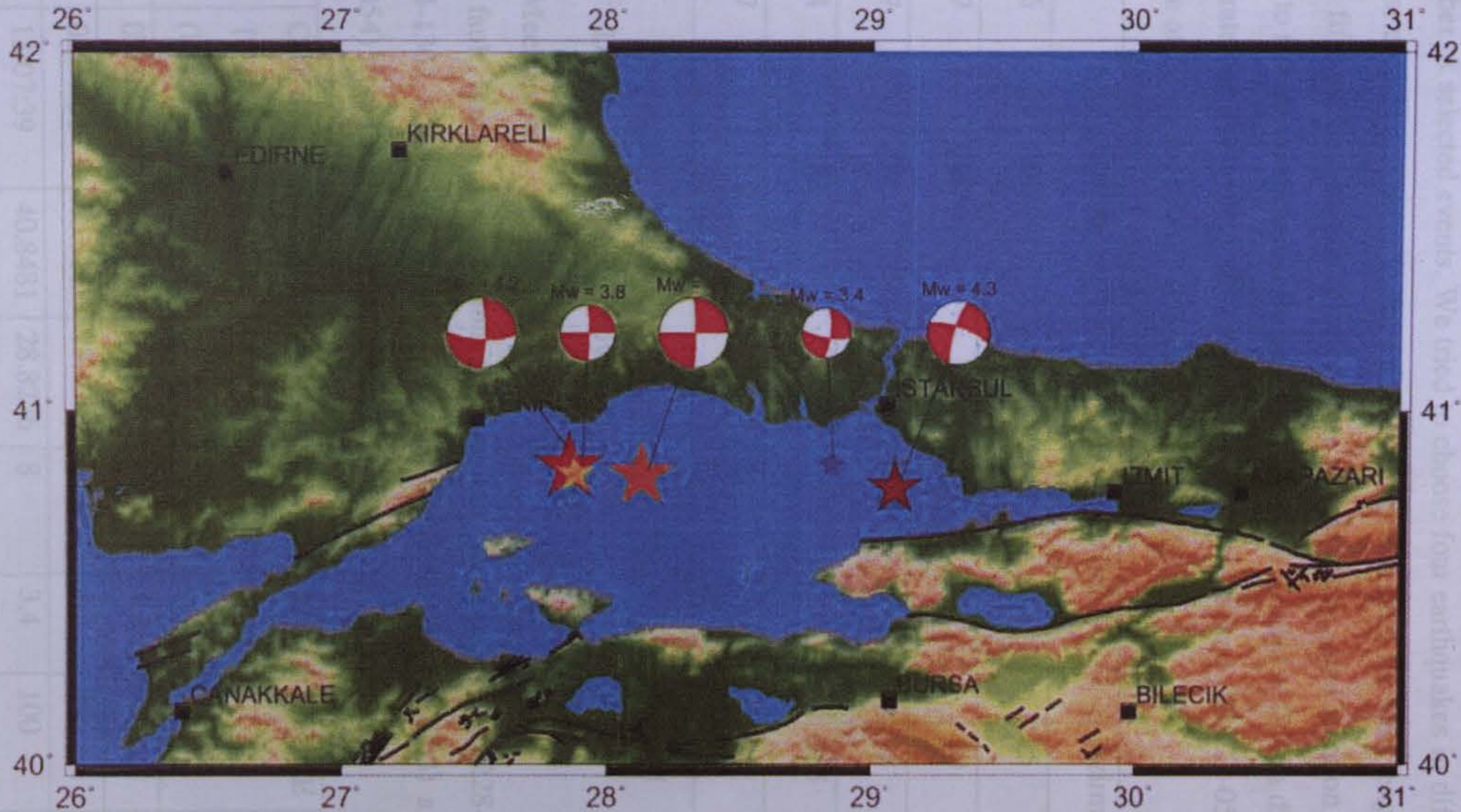

Figure 3.2 Selected earthquakes with lower hemisphere projections of the focal mechanism on the reflief map of Marmara Region

fault, and most of the earthquakes are too small in magnitude and have no solution for their fault planes. Finally even if there are enough earthquakes the computation time required would be too high to be handled in this thesis. Therefore we have applied the method only on a small number of selected events. We tried to choose four earthquakes in different locations along the Marmara Sea in order to have a representative model for total length of the future rupture. The fifth earthquake was selected more or less at the same location as the previous one in order to test the consistency. Broadband data were recorded at ISK in digital form at 50 Hz sample rate for the events 020228-0837, 020323-0236 and 020323-0538 and with a sampling rate of 20 Hz for 990817-0554 and 010324-1307.

Earthquake	Station	Distance (km)	Azimuth(degree)
020323-0236	ISK	104	75
020228-0837	ISK	83	70
010324-1307	ISK	31	38
990817-0554	ISK	31	355
020228-0837	TER	125	74

Table 3.3 Distance and Azimuth coverage.

III.8 Focal Mechanism

The fault mechanism solution for the four earthquakes (020228-0837, 020323-0236,010324-1307, 020323-0538) is taken from Ozalaybey et al (2003) and the last one (19990817-054) from the Orgulu (2002).

NO	DATE	ORİGİN TİME (hr mn ss)	LAT(N) (deg)	LON(E) (deg)	DEPTH	Mw	STRİKE	DİP	RAKE
1	020323	02:36:10	40.8418	27.8576	13	4.2	93	75	0
2	020228	08:37:51	40.8165	28.1301	11	4.2	90	90	0
3	010324	13:07:39	40.8481	28.8276	8	3.4	100	75	0
4	020323	05:38:42	40.8231	27.8801	11	3.8	90	90	0
5	990817	05:54:43	40.7812	29.0882	9	4.3	290	74	0

Table 3.4 Location and source parameters of the 5 earthquakes.

These authors have estimated the focal mechanism using both first motion and waveform modeling.

The fault plane solution taken from Orgulu (2002) is based on the Regional Moment Tensor inversion method. In recent years, by taking the advantage of high quality broadband waveform recorded at regional distances, moment tensor solutions are extracted for events of $M \geq 4.0$ (Zhao and Helmberger, 1994). The inversion is based on the linear relationship between waveforms and the five elements of the moment tensor (Dreger and Langston, 1995). Frequency wave-number integration method given by Bouchon (1981) was used to compute Green's functions for local and regional paths between source and stations. Waveform inversion solutions were also verified by the P wave first motions analysis where the reliability depends critically on the azimuthally coverage of the network and the detailed knowledge of crustal structure.

CHAPTER IV

DISCUSSIONS

In the present study, I accepted an average crustal thickness of 35 km, which is close to the ones proposed in previous studies (e.g. 32 km by Bekler, 2002). In any case the few km difference in Moho depth does not change much the shape of the waveform. I represent the crustal velocity structure by constructing a 5-layered model. The thickness of each layer is held fixed (2, 6, 14, 13 km and half medium below Moho) while the P and S velocities are changed sequentially at each step. The tables show us the optimum P, S velocities (in Km/s) and the corresponding correlation coefficient according to the method that I have used. The notation that is use is Vp for P-wave velocity at i^{th} layer, where i changes from 1 to 5.

ISK RECORDING OF 20020323-0236 EARTHQUAKE:

This earthquake is 104 km distance from ISK station. The magnitude is 4.2. I observed enough large energy on the transversal component. There is a good correlation between transversal and vertical components of real and synthetic seismograms. However radial component is less alike. The result is still acceptable because the transversal component has significantly larger energy than the other components and therefore has more weight. For this earthquake high frequency limit is 0.6 Hz while low frequency limit is 0.05 Hz. I used 20 s time window length to calculate the correlation coefficient. However, I use a longer window length for displaying the unfiltered seismograms. In this example, I see a comparatively large amplitude at the transversal component for the complete unfiltered data in the synthetic seismogram. This may be due to the fact that the station is located nearly at the nodal plane which amplifies the transversal component. In real life such ideal situation do not exist because there is always some 3-dimentional disturbances. Therefore I do not see the same effect in the observed data.

Correlation V,R,T	Vp1,Vs1	Vp2,Vs2	Vp3,Vs3	Vp4,Vs4	Vp5,Vs5
0.27-0.39-0.21	2.0,1.1	5.4,3.0	6.3,3.6	7.1,4.1	7.7,4.4

Table 4.1 Optimum P, S velocity and correlation coefficients of 200323-0236(ISK).

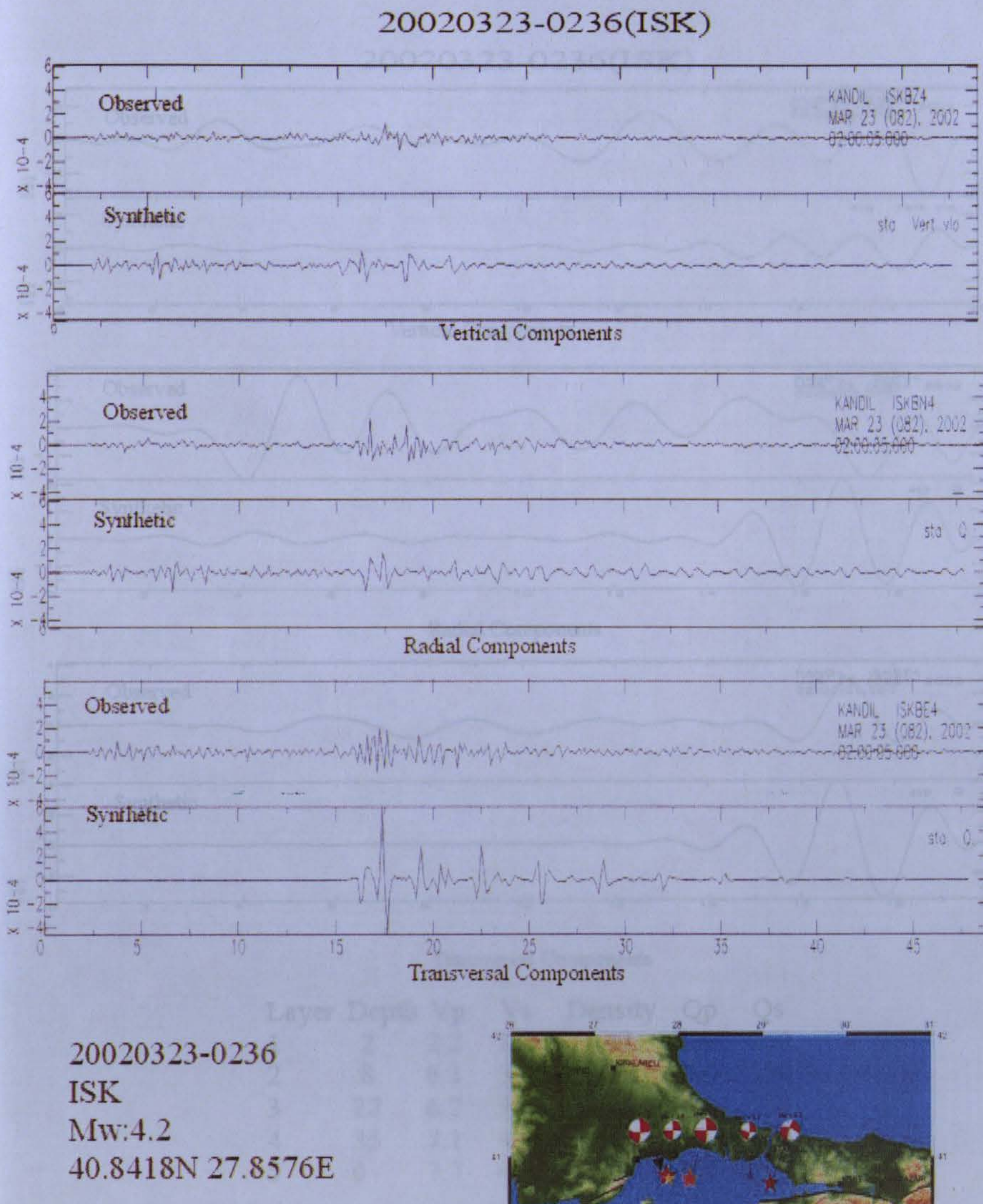

20020323-0236
ISK
Mw:4.2
40.8418N 27.8576E

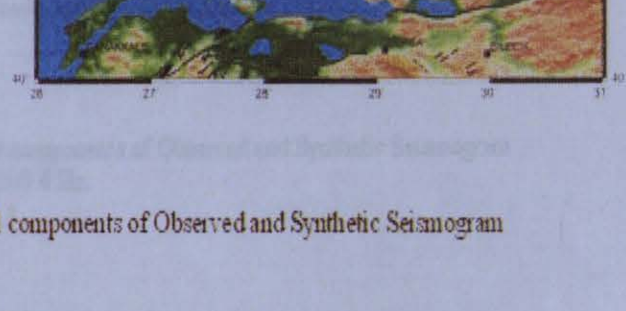

Figure 4.1 Vertical,Radial and Transversal components of Observed and Synthetic Seismogram

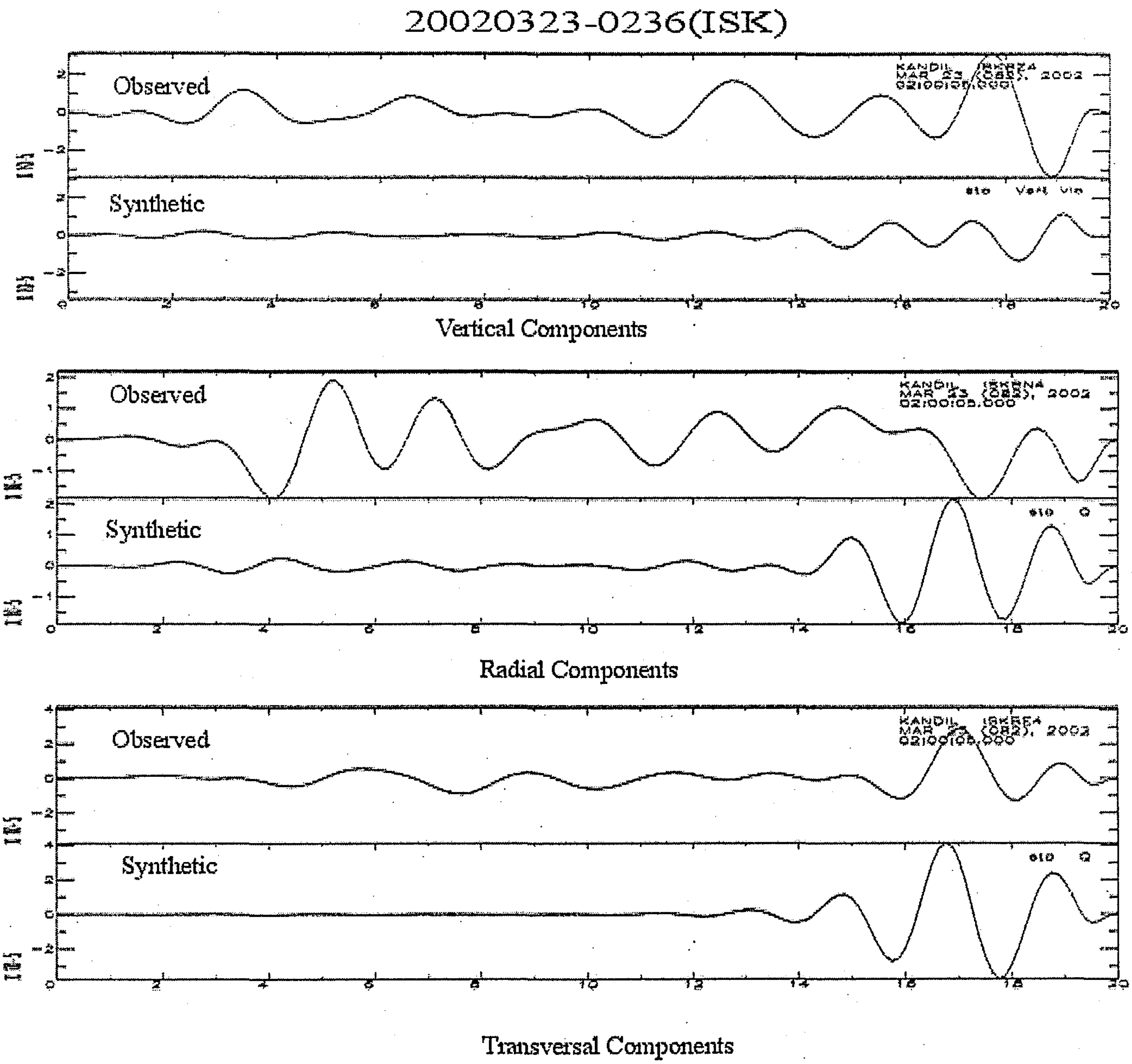

Layer	Depth	Vp	Vs	Density	Qp	Qs
1	2	2.2	1.2	1.47	300	150
2	8	6.1	3.4	2.72	300	150
3	22	6.2	3.5	2.75	300	150
4	35	7.1	4.1	3.02	300	150
5	0	7.7	4.4	3.23	300	150

Contents of input file

Figure 4.2 Vertical,Radial and Transversal components of Observed and Synthetic Seismogram
Traces are filtered between 0.05-0.6 Hz.

20020323-0236(ISK)

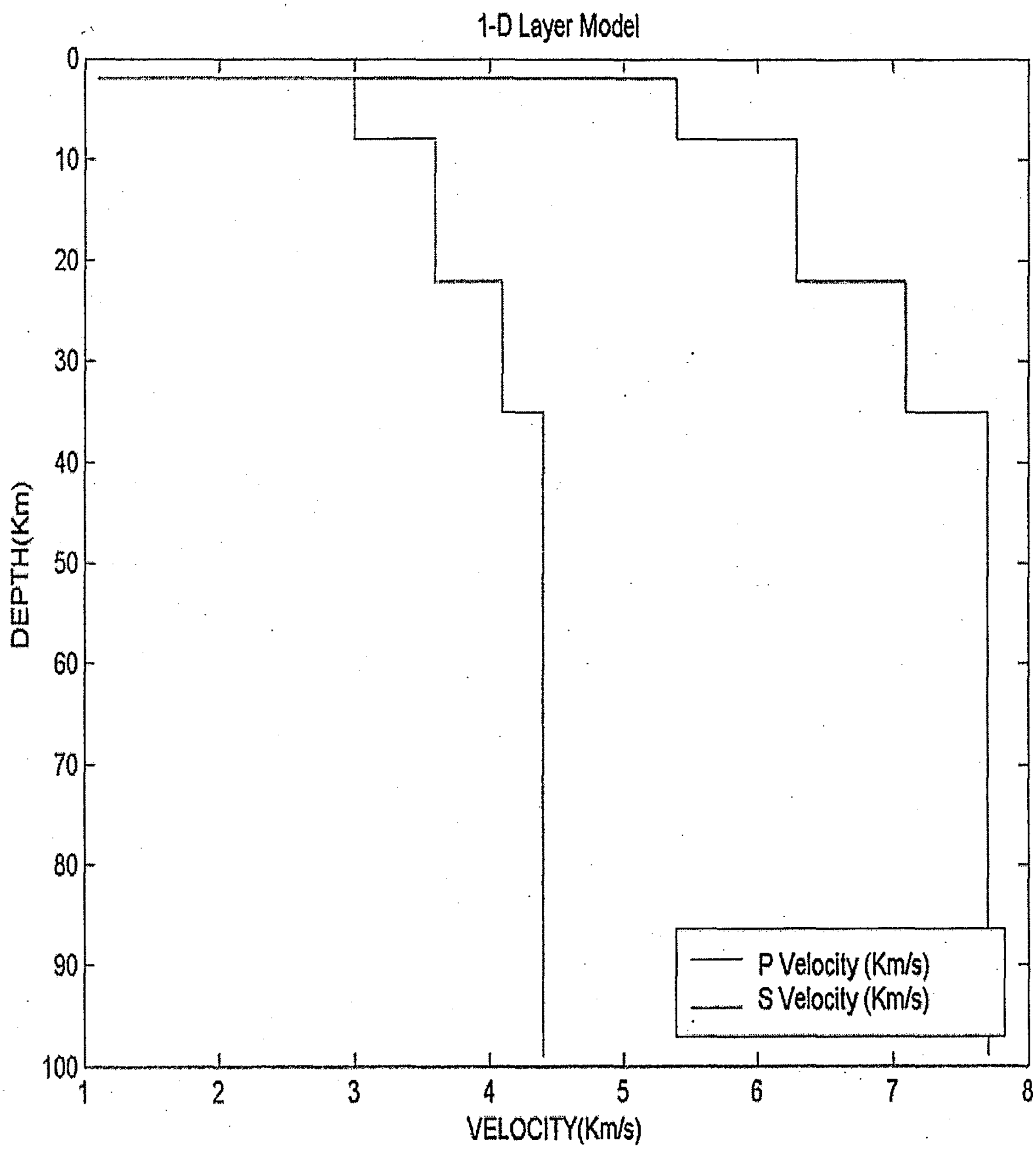

Figure 4.3 P and S wave crustal velocity models for 20020323-0236 earthquake.

ISK RECORDING OF 19990817-0554 EARTHQUAKE:

This earthquake is 31 km from the ISK station and therefore one of the nearest event to be studied. The magnitude is 4.3. I can observe relatively good fitting for P-wave section of the vertical and radial components and S-wave section of the transversal component. This means that the fitting starts to fail in the part of the waveform where 3-dimentional effect starts to dominate. Similar to the previous case, large amplitude in the transversal component due to nodal plane is over emphasized in the synthetic case. For this earthquake high frequency limit is 0.8 Hz and the low frequency limit is 0.05 Hz.

Correlation V,R,T	**Vp1,Vs1**	**Vp2,Vs2**	**Vp3,Vs3**	**Vp4,Vs4**	**Vp5,Vs5**
0.31-0.21-0.31	2.4,1.4	4.7,2.7	6.2,3.5	7.3,4.1	7.7,4.4

Table 4.3 Optimum P, S velocity and correlation coefficients of 19990817-0554 (ISK).

19990817-0554(ISK)

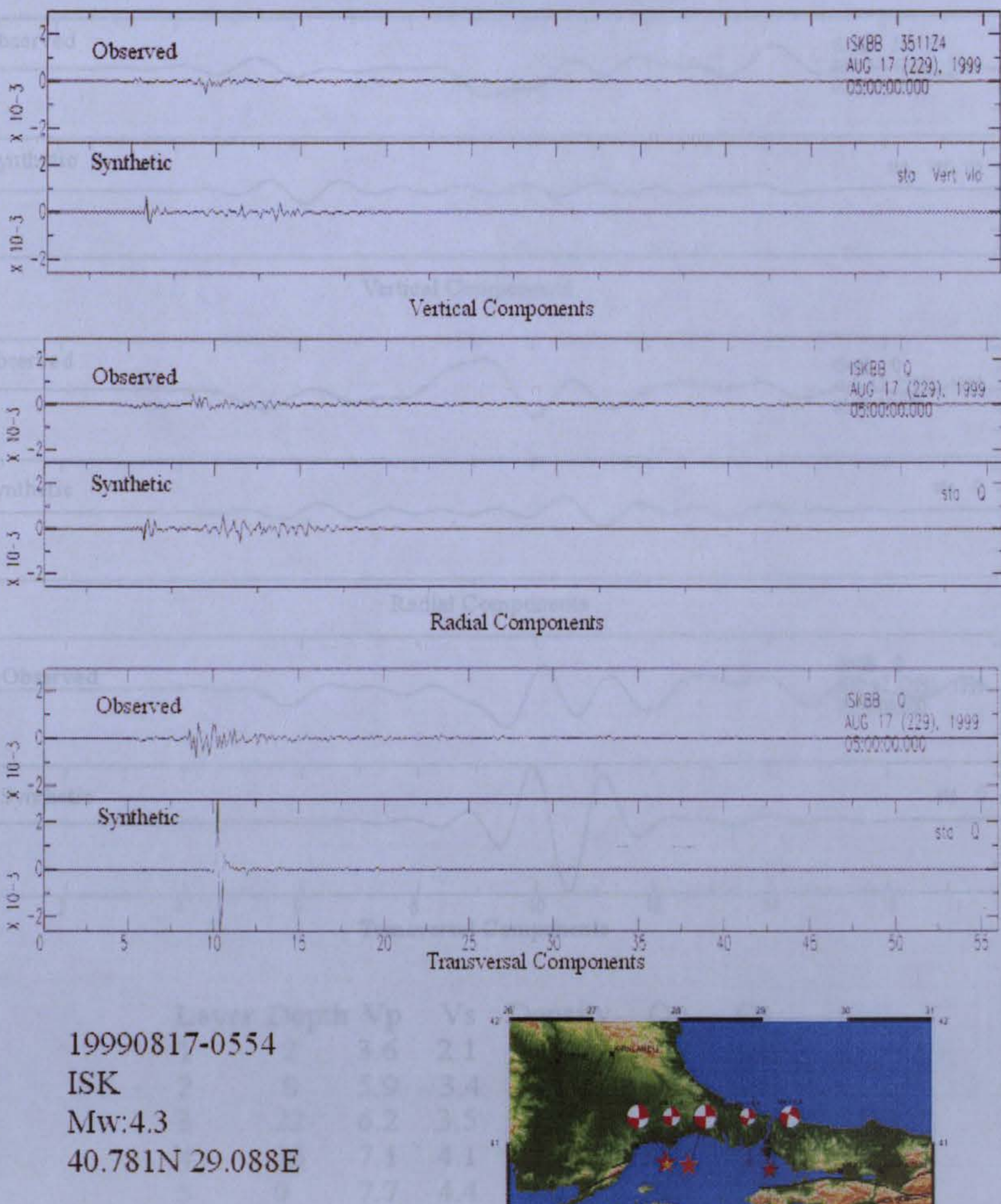

19990817-0554
ISK
Mw:4.3
40.781N 29.088E

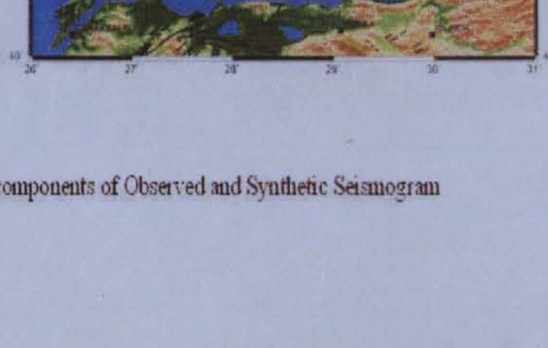

Figure 4.4 Vertical,Radial and Transversal components of Observed and Synthetic Seismogram

19990817-0554(ISK)

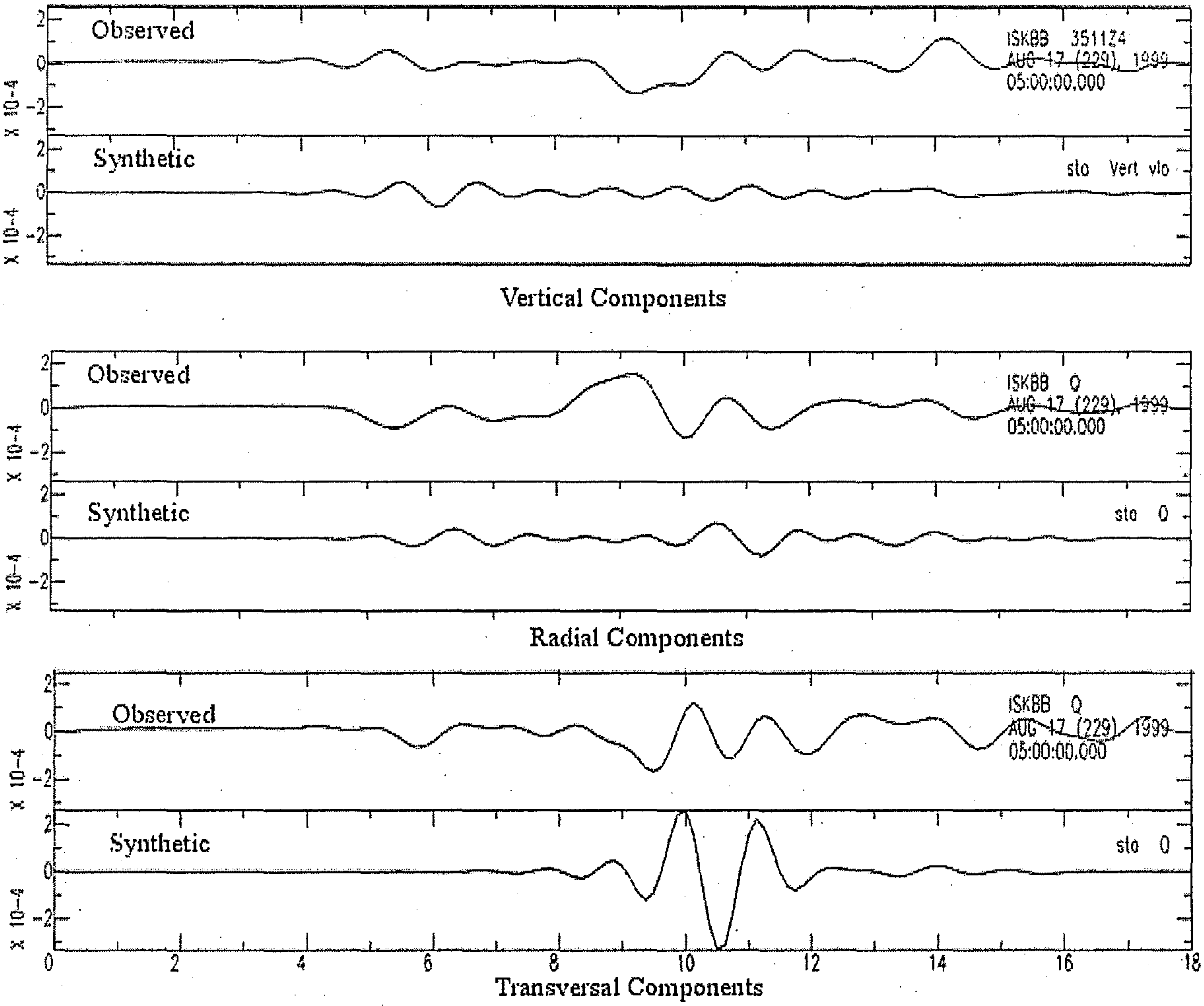

Layer	Depth	Vp	Vs	Density	Qp	Qs
1	2	3.6	2.1	1.92	300	150
2	8	5.9	3.4	2.65	300	150
3	22	6.2	3.5	2.75	300	150
4	35	7.1	4.1	3.04	300	150
5	0	7.7	4.4	3.23	300	150

Contentes of input file

Figure 4.5 Vertical,Radial and Transversal components of Observed and Synthetic Seismogram
Trace are filtered between 0.05-1.0Hz.

19990817-0554(ISK)

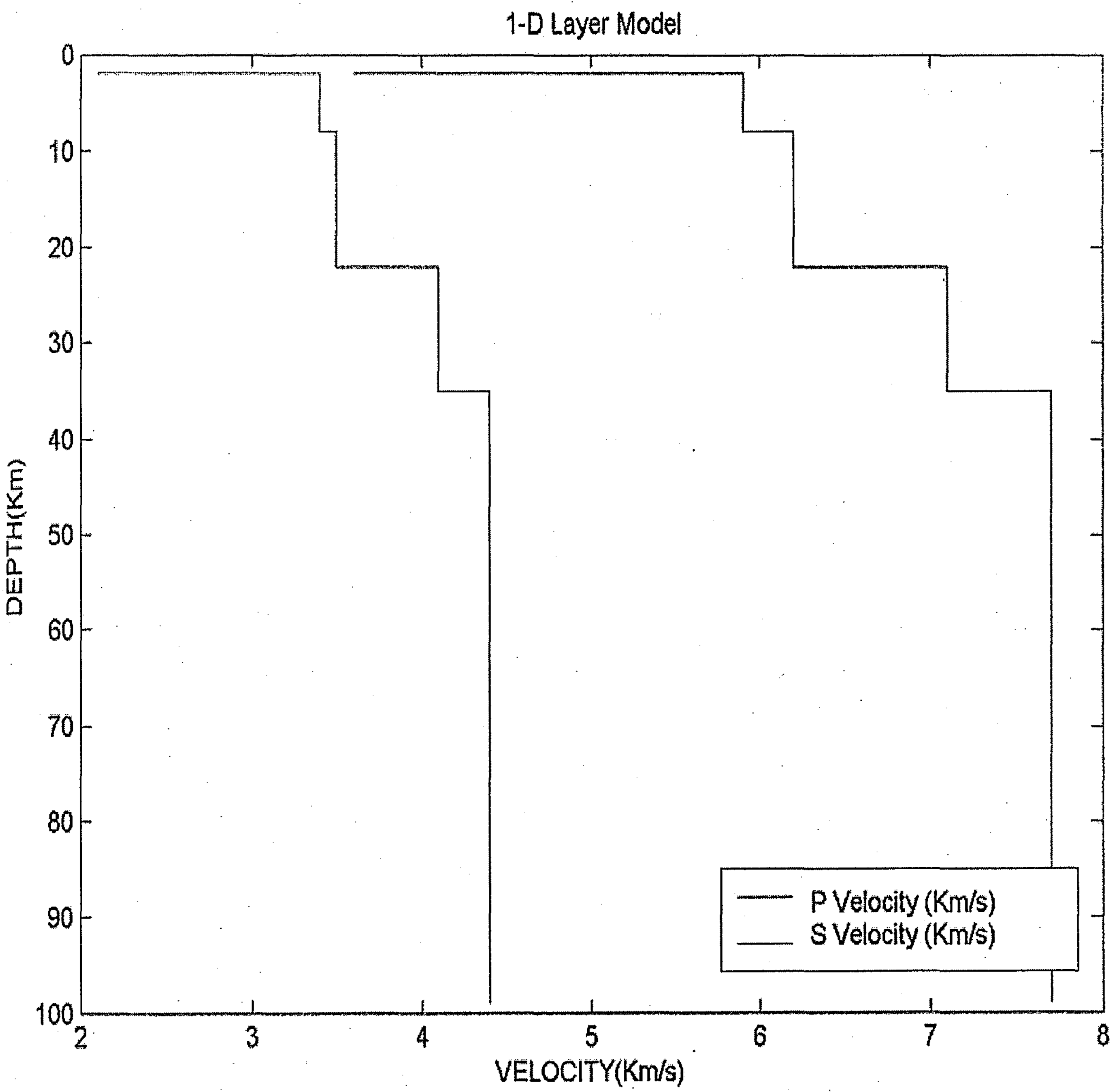

Figure 4.6 P and S wave crustal velocity models for 199908-0554 earthquake.

ISK RECORDING OF 20010324-1307 EARTHQUAKE:

This earthquake is 31 km far from the ISK station. The location of the earthquake is very close the ISK. The magnitude is 3.4. Because of that reason the record is noisier as compared to others. I there am a good fitting for the radial and the transversal components. For this earthquake we observe that the unfiltered waveform also show quite good resemblance. The vertical component which has a weaker fit has also the weakest energy which means that it is relatively less significant. It is to be noted that, in order to have a good fit, I had to increase the S-velocities in this model to relatively higher value as compared to the others examples. Can it be related to the short distance of the epicenter which means that only the upper crustal layers become significant, is still an open question. For this earthquake high frequency limit is 1.0 Hz, low frequency limit is 0.2 Hz.

Correlation V,R,T	Vp1,Vs1	Vp2,Vs2	Vp3,Vs3	Vp4,Vs4	Vp5,Vs5
0.21-0.34-0.10	1.6,1.2	4.7,3.2	6.2,4.0	7.1,4.2	7.7,4.4

Table 4.4 Optimum P, S velocity and correlation coefficients of 20010324-1307 (ISK).

20010324-1307(ISK)

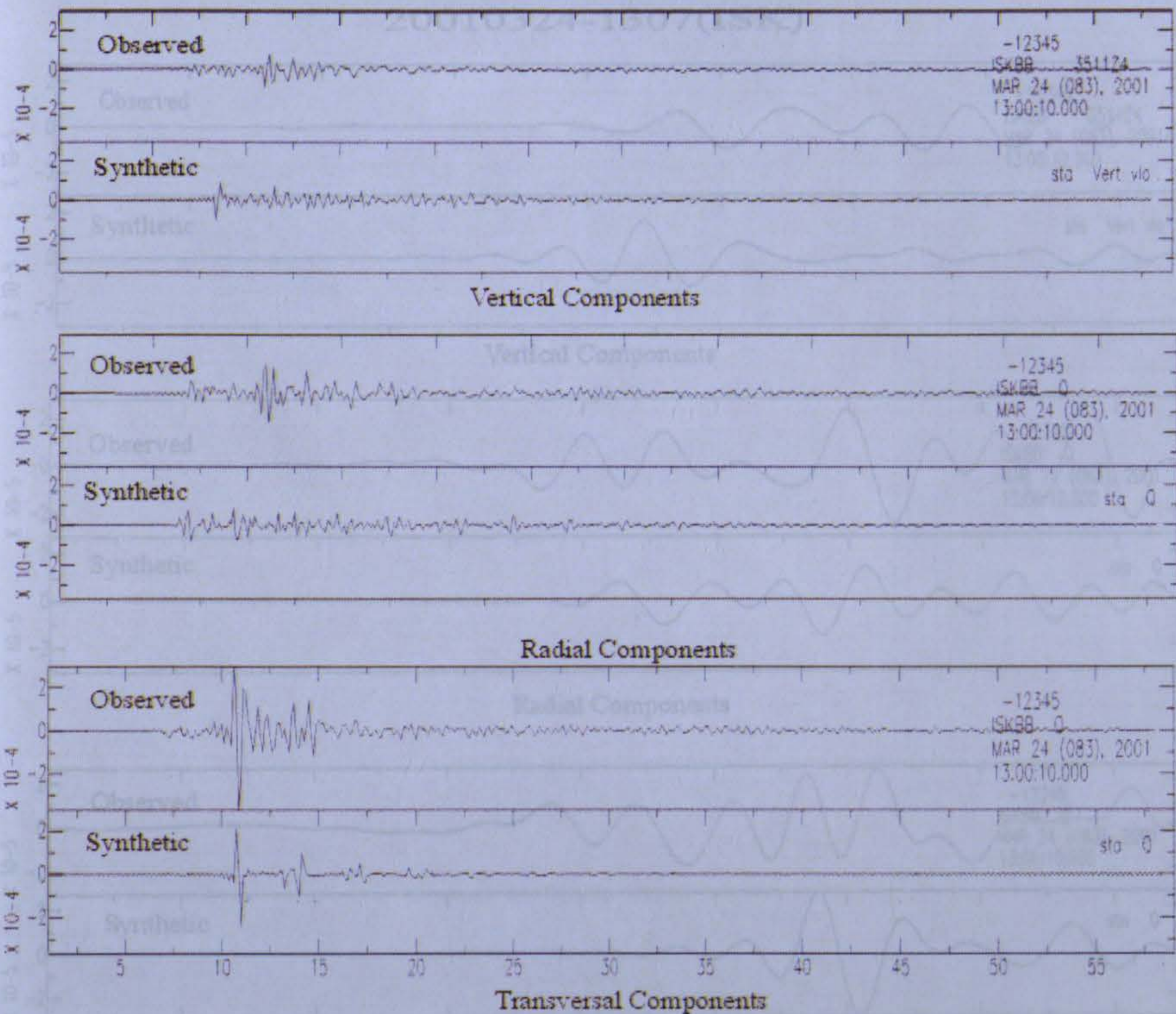

20010324-1307
ISK
Mw:3.4
40.8481N 28.8276E

Figure 4.7 Vertical,Radial and Transversal components of Observed and Synthetic Seismogram

20010324-1307(ISK)

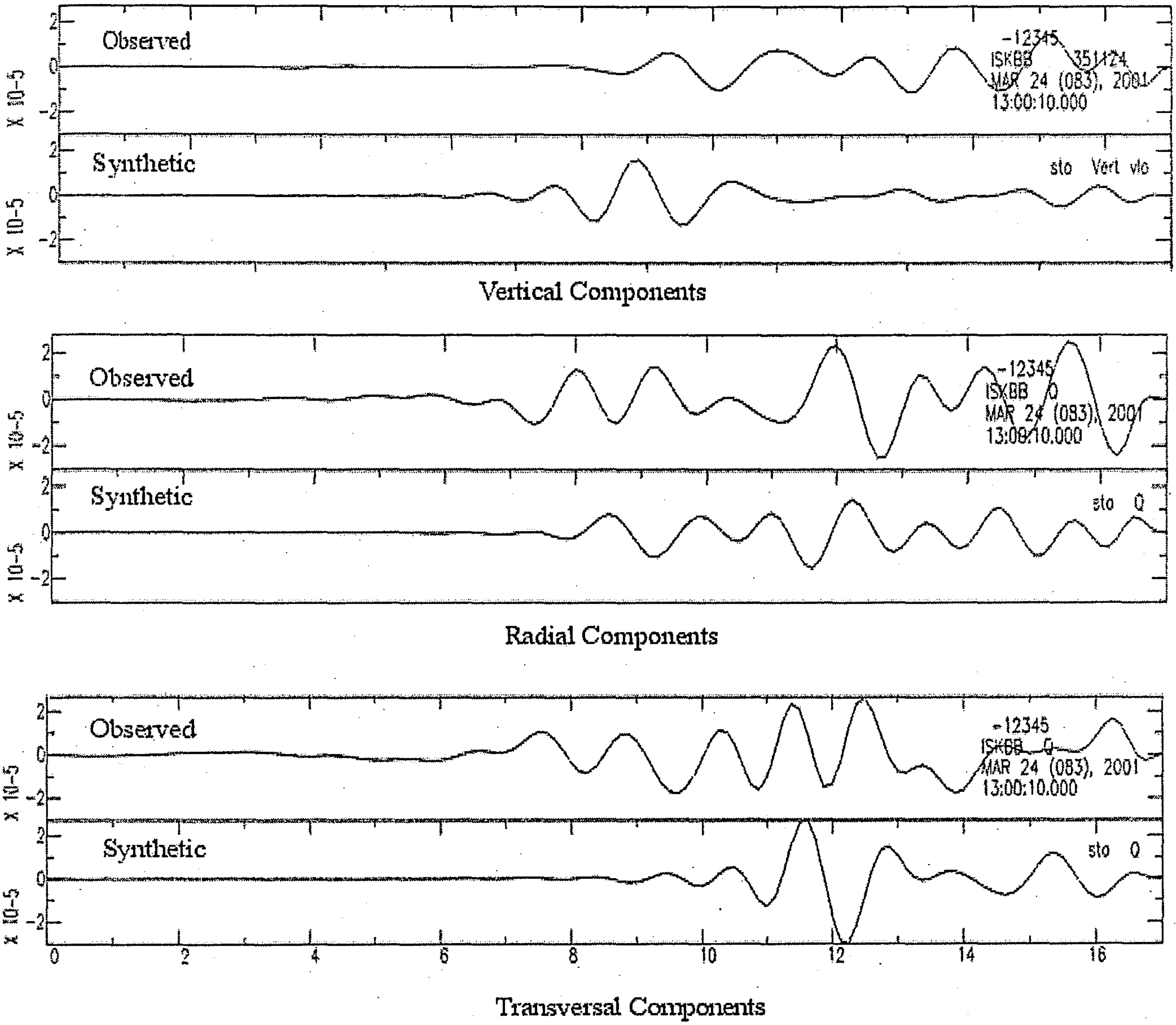

Layer	Depth	Vp	Vs	Density	Qp	Qs
1	2	1.6	1.2	1.28	300	150
2	8	4.7	3.2	2.27	300	150
3	22	6.2	4.0	2.75	300	150
4	35	7.1	4.2	3.04	300	150
5	0	7.7	4.4	3.23	300	150

Contents of input file

Figure 4.8 Vertical,Radial and Transversal components of Observed and Synthetic Seismogram
Trace are filtered between 0.2-1.0 Hz.

20010324-1307(ISK)

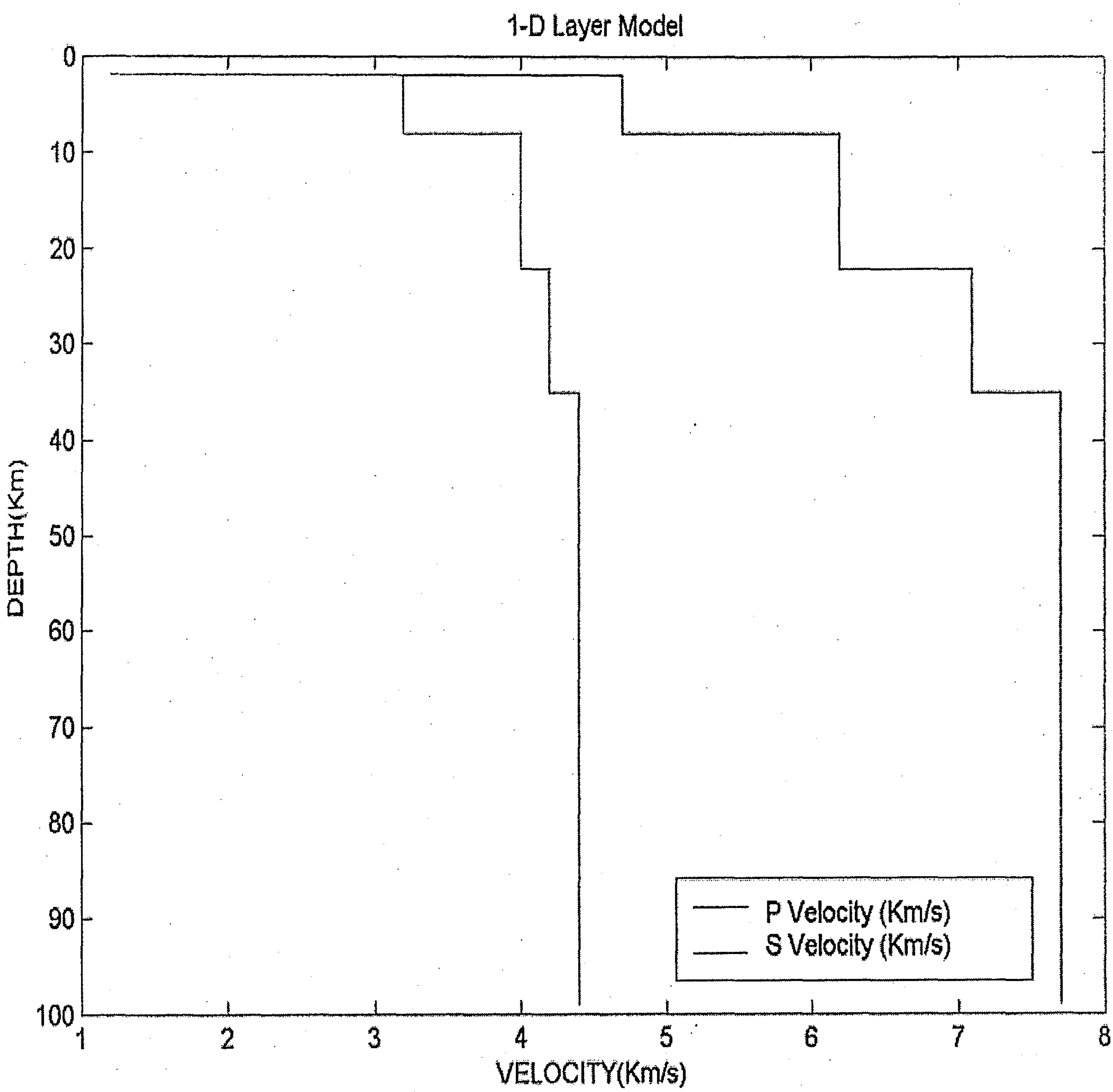

Figure 4.9 P and S wave crustal velocity models for 20010324-1307 earthquake.

TER RECORDING OF 20020228-0837 EARTHQUAKE:

This earthquake is 125 km distance from the TER station. The magnitude is 4.2. I can observe good fitting for all components. The same earthquake was also analyzed by Ozalaybey et al (2003) which also obtained good fitting between all components, mainly the vertical and the transversal. It is surprising to note that the unfiltered waveforms do not show the same correlation, which means that the crustal model obtained do not represent well the high frequency contributions from the ray path. For this earthquake high frequency limit is 0.8 Hz, low frequency limit is 0.05 Hz.

Correlation V,R,T	Vp1,Vs1	Vp2,Vs2	Vp3,Vs3	Vp4,Vs4	Vp5,Vs5
0.29-0.51-0.45	2.2,1.3	5.4,3.1	6.4,3.7	7.1,4.1	7.7,4.4

Table 4.5 Optimum P, S velocity and correlation 20020228-0837 (TER).

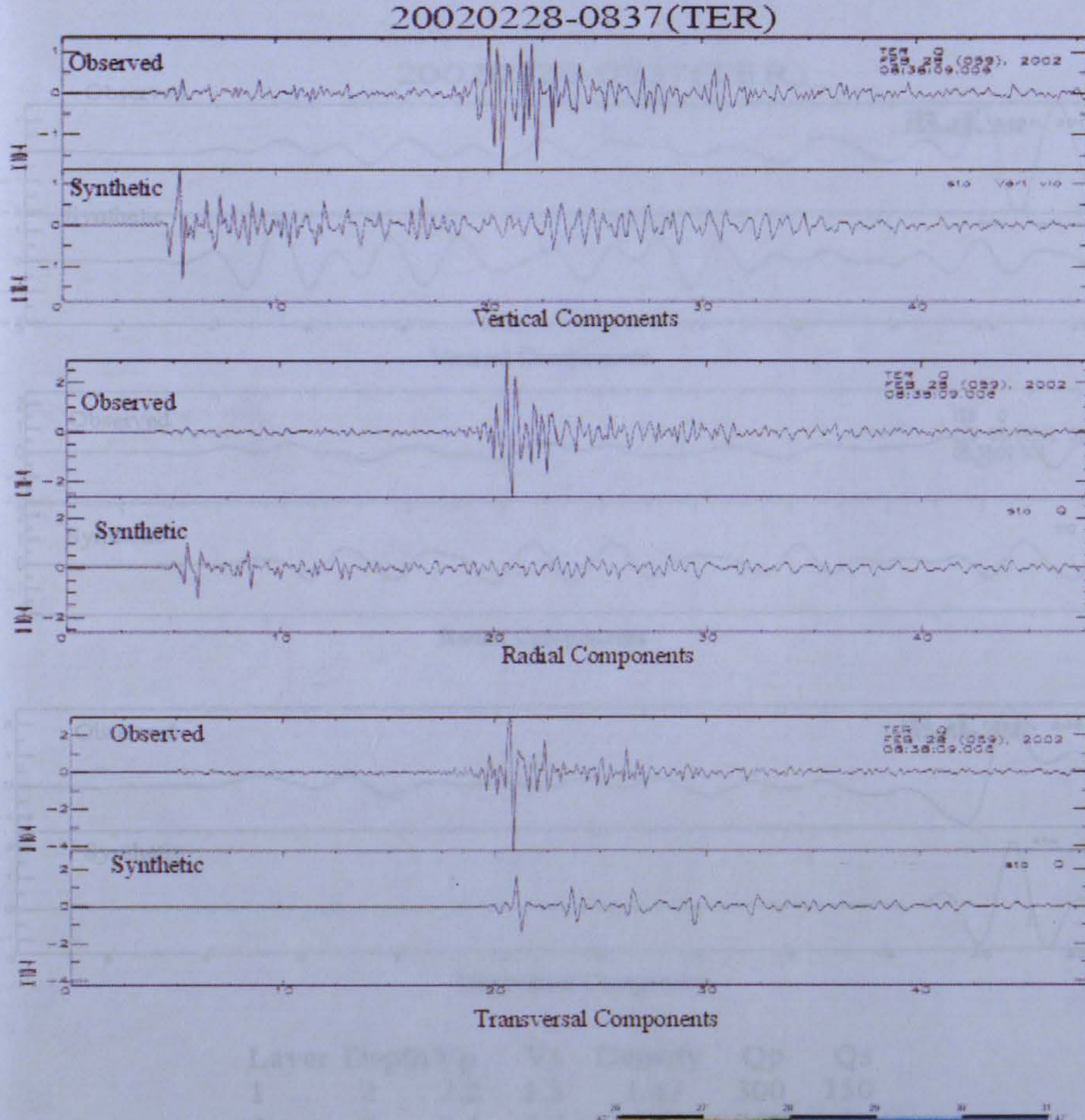

20020228-0837
TER
Mw:4.2
40.8165N 28.1301E

Figure 4.10 Vertical Radial and Transversal components of Observed and Synthetic Seismogram

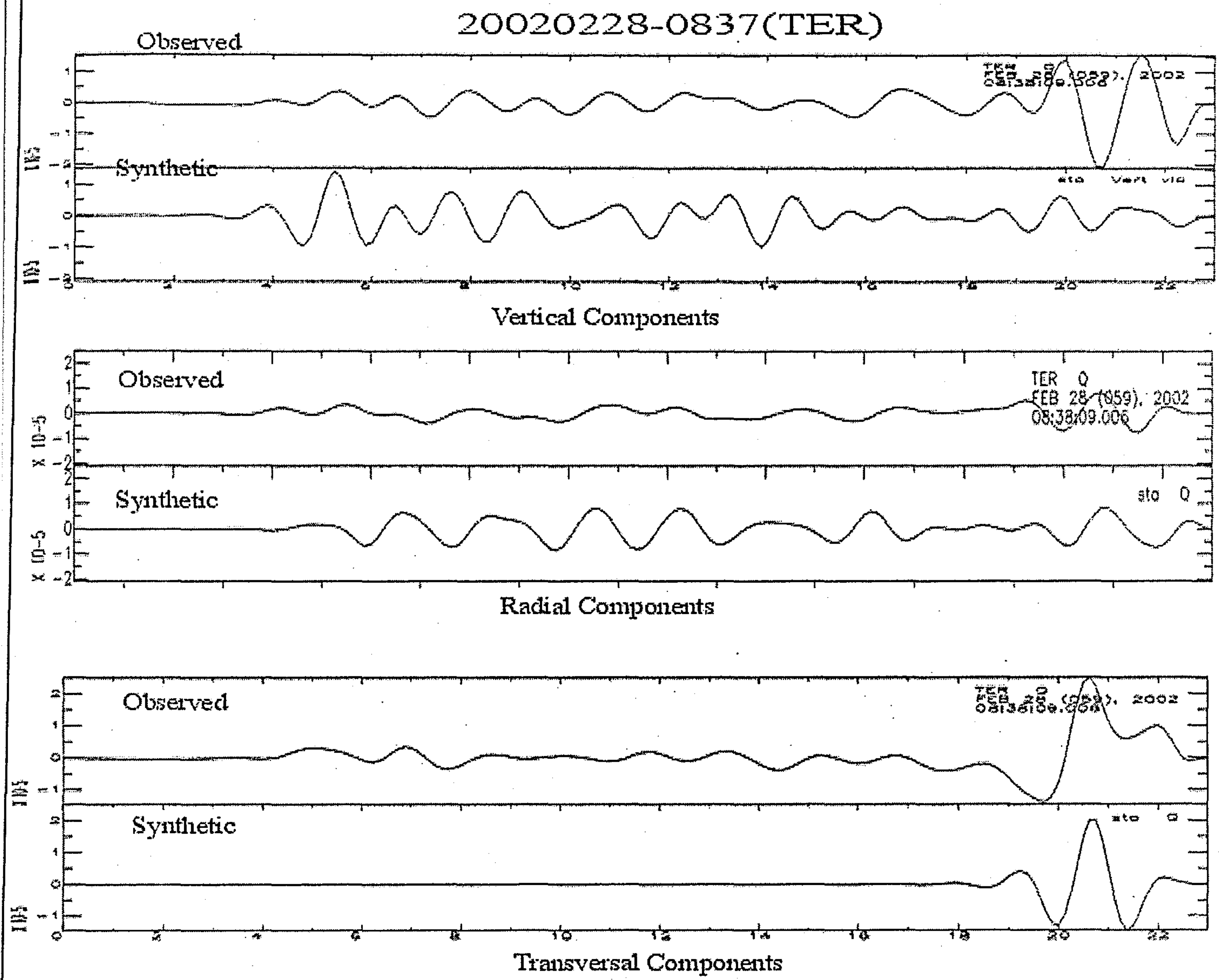

Layer	Depth	Vp	Vs	Density	Qp	Qs
1	2	2.2	1.3	1.47	300	150
2	8	5.4	3.1	2.49	300	150
3	22	6.4	3.7	2.82	300	150
4	35	7.1	4.1	3.04	300	150
5	0	7.7	4.4	3.23	300	150

Contents of input file

Figure 4.11 Vertical,Radial and Transversal components of Observed and Synthetic Seismogram
Traces are filtered between 0.05-0.8 Hz.

20020228-0837(TER)

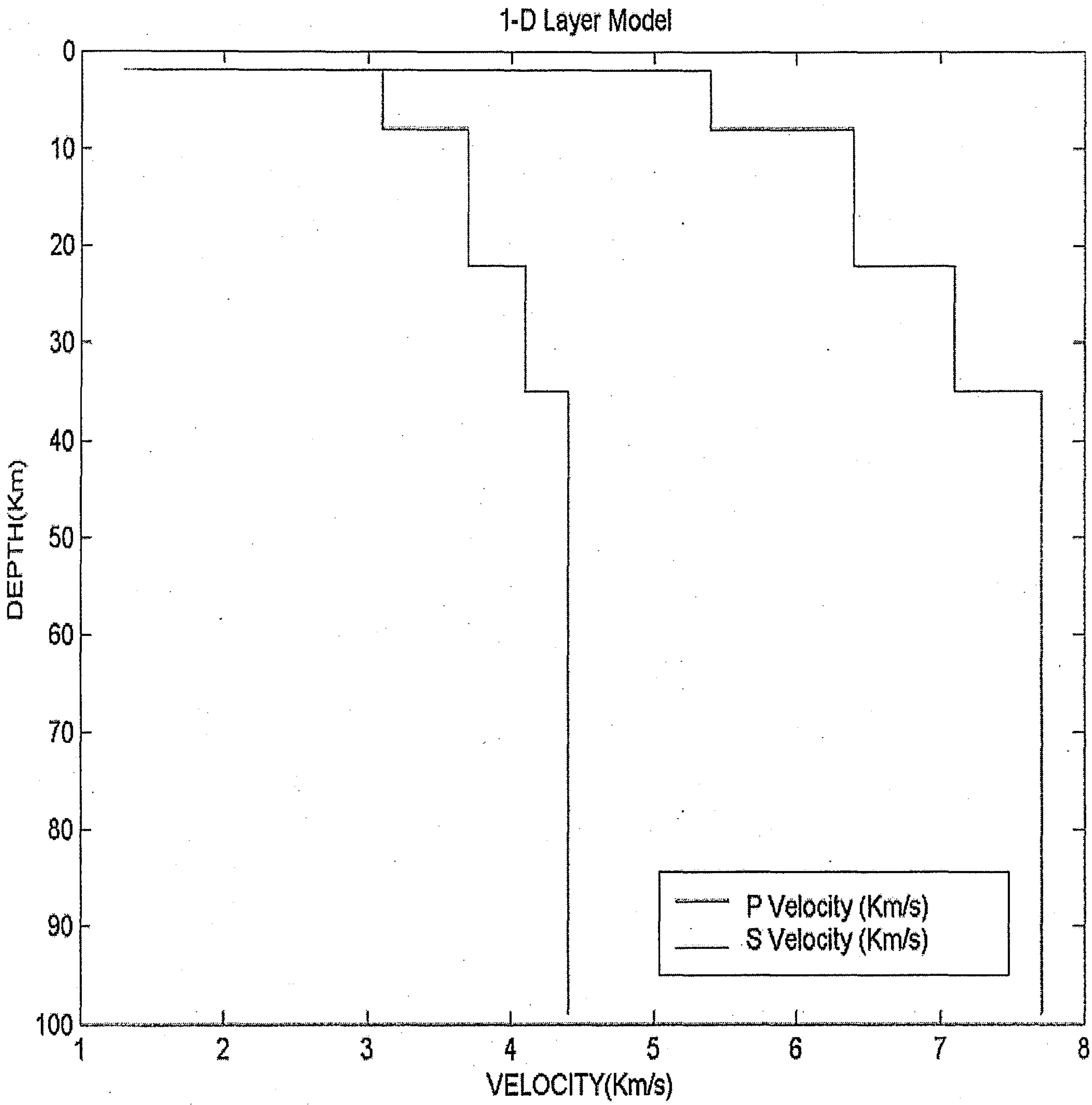

Figure 4.12 P and S wave crustal velocity models for 20020228-0837(ter) earthquake.

ISK RECORDING OF 20020228-0837 EARTHQUAKE:

This earthquake is the same as the previous one and is 83 km far from the ISK station. I can observe good fitting for radial and vertical components. On the other hand I observe a moderate fitting for the transversal component. For this earthquake high frequency limit is 1.0 Hz, low frequency limit is 0.4 Hz. It is to be noted that the correlation coefficients are different for ISK and TER stations, even if the same earthquake and more or less the same azimuth are used. Noise level of ISK station is probably higher then TER station which is located in a remote location. Finally, it may be also true that ISK station suffers more from 3-dimentional effects as compared to TER station.

Correlation V,R,T	Vp1,Vs1	Vp2,Vs2	Vp3,Vs3	Vp4,Vs4	Vp5,Vs5
0.27-0.31-0.32	1.2,0.7	4.7,2.8	6.7,3.8	7.4,4.4	8.0,4.7

Table 4.6 Optimum P, S velocity and correlation 20020228-0837 (ISK).

20020228-0837(ISK)

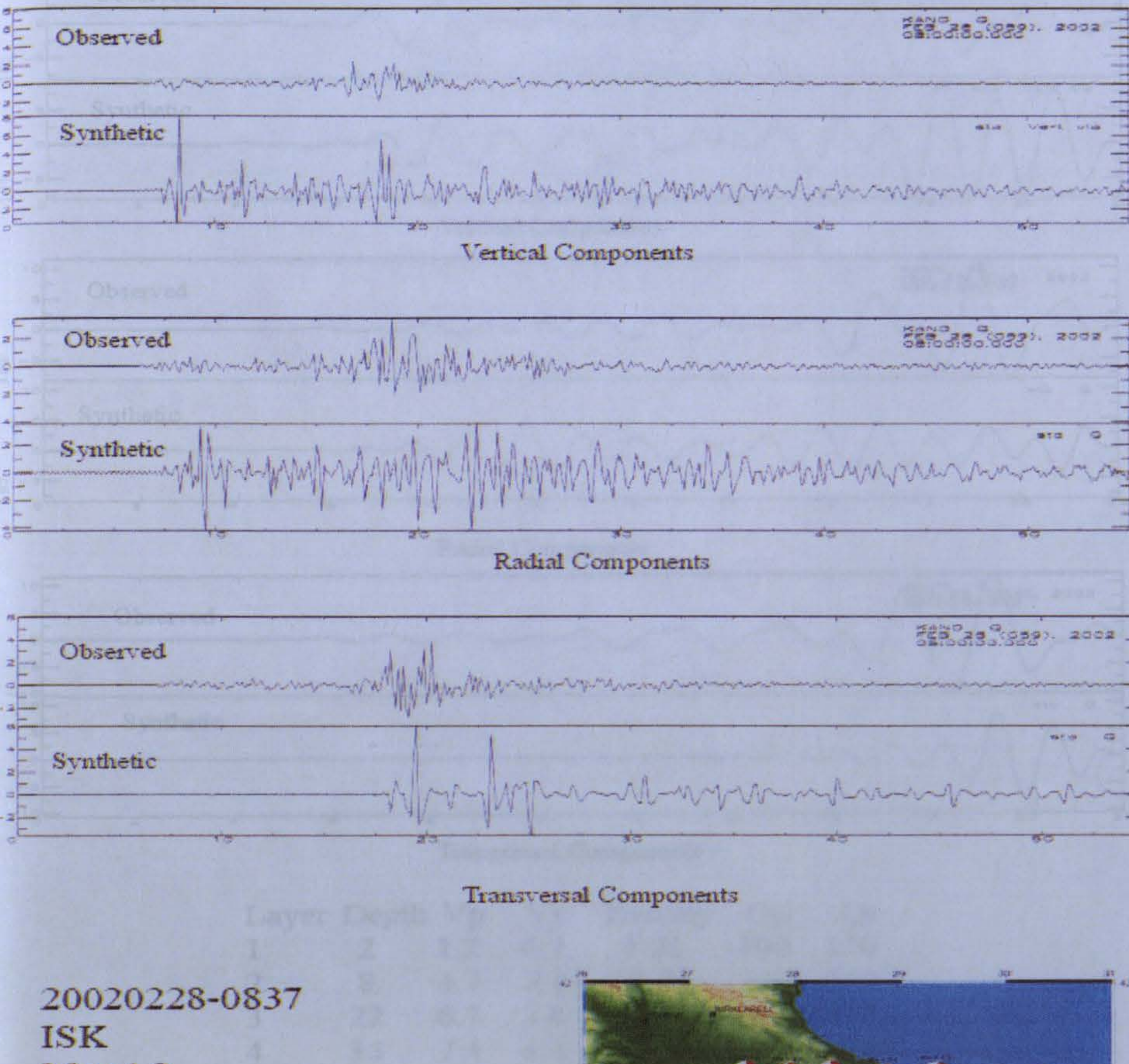

Transversal Components

20020228-0837
ISK
Mw:4.2
40.8165N 28.1301E

Figure 4.13 Vertical,Radial and Transversal components of Observed and Synthetic Seismogram

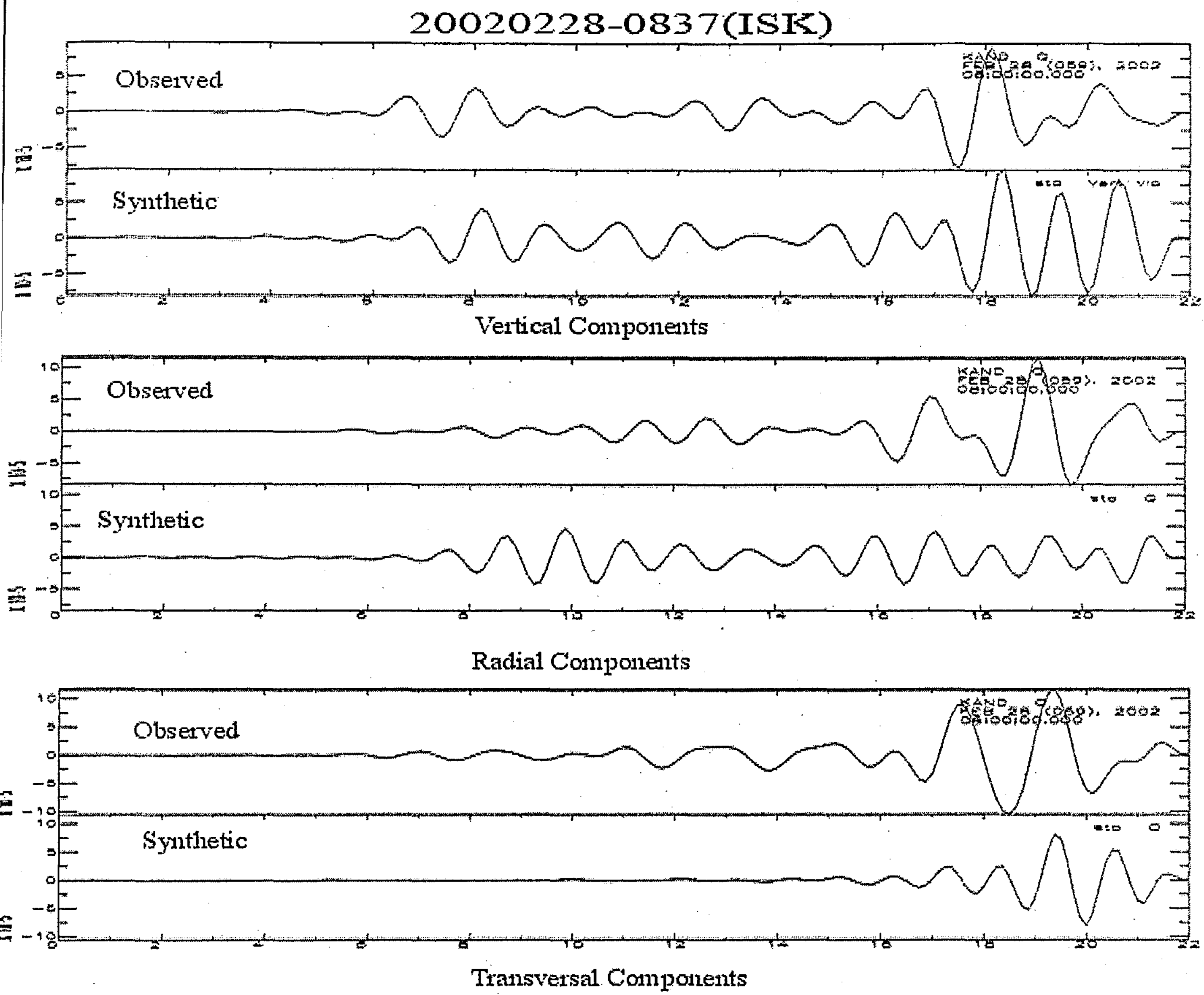

Layer	Depth	Vp	Vs	Density	Qp	Qs
1	2	1.2	0.7	1.21	300	150
2	8	4.7	2.8	2.40	300	150
3	22	6.7	3.8	2.78	300	150
4	35	7.4	4.4	3.18	300	150
5	0	8.0	4.7	3.33	300	150

Contents of input file

Figure 4.14 Vertical,Radial and Transversal components of Observed and Synthetic Seismogram
Traces are filtered between 0.4-1.0 Hz.

20020228-0837(ISK)

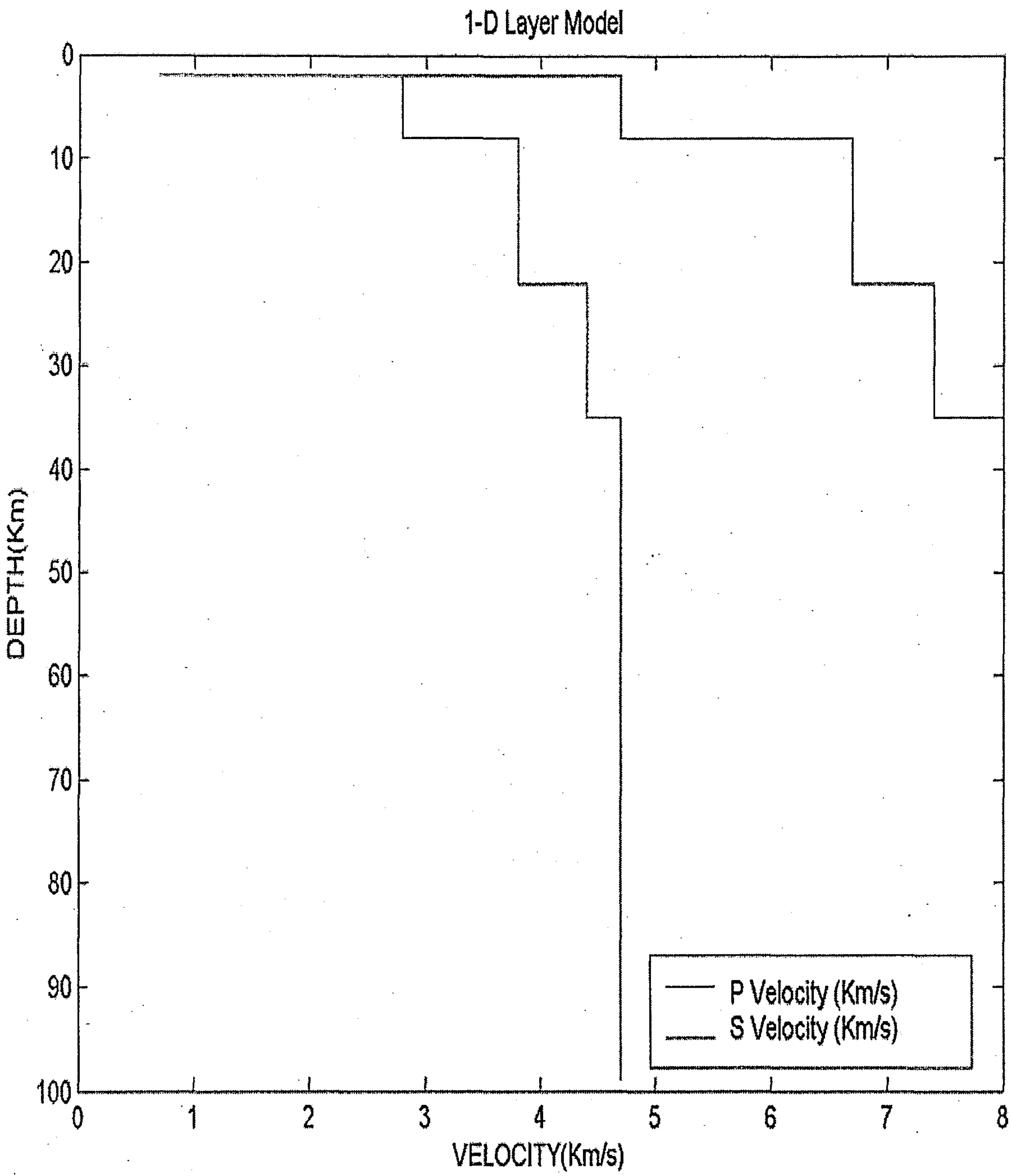

Figure 4.15 P and S wave crustal velocity models for 20020228-0837(ISK) earthquake.

CHAPTER V

CONCLUSION

Estimates of expected ground motion at a given distance from an earthquake of a given magnitude are fundamental inputs to earthquake hazard assessments. In practice the full description of the ground motion is seldom used, only peak ground acceleration values (PGA) goes into design criteria. A single scalar value such as the PGA is too much restricted to give a full description of the true ground motion. Recently, the synthetic seismogram modeling is readily available as an important tool to be used in more realistic description of the ground shake. This is successfully used in seismic hazard studies.

The performance of any type of synthetic seismogram generation depends entirely on how well the crustal structure is known. The conventional methods to be used for examining the crustal structure such as refraction and reflection require extensive field studies and costly data collecting campaigns. However, seismic hazard assessment does not require a very detailed description of the crust. Since there is no intention of any geological interpretation, a simple coarse model is enough to generate useful seismograms. For that purpose a simpler approach is applied which uses seismograms from earthquakes occurring along the future rupture zone. Once the fault plane solution is known the velocity structure can be approximated by simple layered model. Consequently any type of rupture complexity can then be solved as a forward problem.

The velocity structure of the crust in the Sea of Marmara is investigated using Discrete Wave number Technique (Bouchon, 1981), which allows the construction of layered earth model by synthetic seismogram modeling. To apply the method it is not necessary to collect large amount of data, which would require costly operations such as refraction line or marine seismic surveys. This is a simple method, which only requires the use of computer and a number of high quality earthquakes recordings. The results that are obtained are sufficient to provide enough accuracy for a realistic estimation of the ground motion that is expected during a destructive earthquake. In this thesis, I have used 5 earthquakes located at different parts of the fault in order to represent the crustal velocity structure with a 5-layered model each.

The main assumption in the Discrete Wave number Technique (Bouchon, 1981) crustal model is the homogeneous velocity in each layer, which is considered to be mainly flat. I cannot observe lateral velocity changes that may occur within a given layer. However using more than one earthquake along the fault, lateral variations are somewhat taken into account.

The method although attractive from the simplicity point of view, does have some disadvantages.

First of all, I need a three component broadband data for detailed waveform modeling. This type of data is not always available within the city metropolitan area. Furthermore, in order to apply the method, there must be adequate number of earthquakes. This condition is also not easily satisfied. Only a certain part of the future rupture zone can be active while the rest can be aseismic, which means that I do not have earthquakes to simulate the waveform. The location of the earthquake need also be known with sufficient accuracy. Finally, a focal mechanism solution must also be estimated before searching the optimal crustal structure. All these conditions are not easily applicable, at least for the case of Istanbul, they are satisfied only with the data collected during the last few years.

Once the data is available there are also difficulties in searching for the optimal velocity structure. In order to get optimum result, all crustal parameters need to be searched simultaneously, such as P and S wave velocities, layer thickness, Qp, Qs, and density of each layer. Furthermore the search for each individual parameter needs to be fine enough. This is a very heavy load as far as the computation time is required.

This requirement for a high computing power obliged us to search only for the optimal P-wave velocities for each layer within specified search interval, keeping all the other parameters fixed. Particularly, the depths of layers were fixed while searching the P wave velocities. After having the optimum P-wave velocities, S-wave velocities were searched for these optimum P-wave velocities. The rest of other parameters were not changed. It is clear that local optimums are searched in this method while global optimums are ignored. This should certainly degrade the overall performance of the method.

The filtering applied to the waveforms is determined by trial and error approach and is not chosen bigger than 1 Hz. This may have the effect of reducing the sensitivity; applying a low pass filter of 1 Hz often eliminated particularly the reflections from shallow interfaces. That limitation is considered to be secondary since most of the hazard estimation studies are done below 1 Hz. I have also reduced our search to only a portion of the waveform. A window, which comprises the whole of P-wave plus only few initial seconds of the S-wave, is taken into account when comparing observed and calculated waveforms. This is also acceptable because the introduction of the S-coda usually introduces too much complexity and fails to provide additional information. In addition to the waveforms, I also tested that calculated travel times do not deviate too much between synthetics and real waveforms. I have noticed that this is not a critical problem because the travel time can be adjusted to fit the real one without too much disturbing the shape of the waveform. Changing the velocities of the deeper layers within an acceptable range does this.

Ideally the optimum value of the correlation coefficient between observed and calculated data should be 1.00. This is never reached. I found the highest transversal component correlation coefficient which is 0.45 and radial component correlation coefficient is 0.51 for TERZILI station. For ISK station transversal component correlation coefficient is 0.32 for 20020228-0837 earthquake (Mw=4. 2). This may be partly due to the noise level of ISK station which is higher then TER station and also 3-dimentional effects. Similarly, for the same earthquake of 20020228-0837, the correlation coefficient of TERZILI station was found to be higher than ISK station value. I must also consider that making a one-dimensional modeling is too much simplification for ISK which should ideally be modeled by the three dimensional case.

Finally, I expect to find the same optimal crustal model for earthquakes that are located next to each other. However, I found different velocities for the first layer from two earthquakes that are located close to each other. This may be a sign of instability in the method.

Despite the problems that are mentioned above, the method is practical and the performance can be improved by the use of better computational algorithms.

The present search algorithm does is a forward algorithm that scans the given parameters in a blind fashion. Naturally the computational burden is immense and only a selected portions of the parameters can be scanned due practical constraints. A more clever search algorithm that uses a feedback mechanism to guide the search in a selective parameter space and accelerates the convergence towards the optimum (such as steepest descent, etc) will allow the scanning of wider range of parameter (eg estimating the layer depths in parallel to velocities, etc). This will certainely give a more optimal result. Finally, modern global optimisation approches such as simulated annealing or genetic algorithms are also expected to give more optimal results.

In any case this method is to be used for hazard estimation and not for geological interpretation. Therefore, for this purpose that does not require high accuracy and sensitivity, the method proposed is a convenient one since it does not require costly data acquisition campaigns and works with existing earthquake data.

REFERENCES

Abrahamson, N., A., and Shedlock, K., M., Overwiev, Seismological Research Letters, Vol. 68, No. 1, 1997.

Aksu, A.A., Calon, T.J., Hiscott, R.N. and Yaşar, D., Anatomy of the North Anatolian Fault Zone in the Marmara Sea, Western Turkey:. Extensional Basins Above a Continental Transfrom, GSA Today, pp. 3-7, 2000.

Aktar, M., Recent Seismicity of the Marmara Sea and its Implications for the Earthquake Hazard in the City of Istanbul RELIEF - Workshop on "Ground motion simulations based on earthquake scenarios along the North Anatolian Fault Zone'', Bergen, Norway , 2003.

Ambraseys, N.N., Some characteristic features of the Anatolian Fault Zone, Tectonophysics, 9, 143-165, 1970.

Ambraseys, N.N. and Finkel, C.F., Long-term Seismicity of Istanbul and of the Marmara Sea region, Terra Nova, 3, 527-539, 1991.

Ambraseys, N.N. and Jackson, J, A., Faulting associated with historical and recent earthquakes in the Eastern Mediterranean region, Geophys. J. Int., 133, 390-406, 1998.

Ambraseys, N.N. and Jackson, J, A., Seismicity of Marmara (Turkey) since 1500, Geophys. J. Int., 141, F1-F6, 2000.

Ambraseys, N.N., The earthquake of 10 July 1894 in the Gulf of İzmit (Turkey) and Its Relation to the earthquake of 17 August 1999, J. Seismology, 5, 117-128, 2001.

Armijo, R., Meyer, B., King, G.C.P., Rigo, A. and Papanastassiou, D., Quaternary Evolution of the Corinth Rift and Its implication for the late Cenozoic Evolution of the Aegean, Geophys. J. Int., 126, 11-53, 1996.

Armijo, R., Meyer, B., Hubert, A., and Barka, A., Westwards Propagation of the North Anatolian Fault into the Northern Aegean: Timing and Kinematics, Geology, 27, 267-270, 1999.

Armijo, R., Meyer, B., Navarro, S., King, G., and Barka, A., Asymmetric Slip Partitioning in the Sea of Marmara pull-apart: A Clue to Propagation Processes of the North Anatolian Fault, TerraNova, 14, 80-86, 2002.

Atakan, K., Ojeda, A., Meghraoui, M., Barka, A., Erdik, M., and Bodare, A., Seismic Hazard in Istanbul following the 17 August 1999 Izmit and 12 November 1999 Düzce Earthquakes, Bull. Seism. Soc. Am., 92, 1.pp, 466-482, 2002.

Barka, A.A., Slip Distribution Along the North Anatolian fault Associated with the Large Earthquakes of the Period 1939 to 1967, Bulletin of the Seismological Society of America, 86, 1238-1254, 1996.

Barka, A.A., Kadinsky-Cade, K., Strike-slip Fault Geometry in Turkey and its influence on earthquake activity, Tectonics, 7, 663-684, 1988.

Bekler, T., Crustal Structure of the Eastern Marmara Region Using Seismic Refraction Experiment and Earthquake Data, Ph.D. Thesis, Bogazici University, 2002.

Boore, D. M., Stochastic Simulation of High Frequency ground motions Based on Seismological Models of the Radiation Spectra, Bulletin of the Seismological Society of America, 73, 1865-1894, 1983.

Bouchon, M., A Simple Method to Calculate Green's Functions for Elastic Layered Media , Bulletin of the Seismological Society of America, Vol.71 , No.4, pp.959-971, 1981.

Bouchon, M., A Review of the Discrete Wavenumber Method, Pure appl.geophys , 160 , 445-465, 2003.

Ergin, M., Aktar M., Biçmen, F., Yörük, A., Yalçın M. N., Kuleli, S., Detailed microearthquake monitoring of the İzmit Bay, Aktif Tektonik Araştırma Grubu-1, 1998.

Flerit, F., Armijo, R., King, G.C.P., Meyer, B., Barka, A., Slip slip partitioning in the Sea of Marmara pull-apart determined from GPS velocity vectors , Geophys.J.Int , 154 , 1-7, 2003.

Gürbüz, C., Aktar, M., Eyidoğan, H., Cisternas, A., Haessler, H., Barka, A., Ergin, M., Türkelli, N., Polat, O., Üçer, S.B., Kuleli, S, Baris, S., Kaypak, B., Bekler, T., Zor, E., Bicmen, F., Yoruk, A. , The Seismotectonics of the Marmara region (Turkey) :results from a microseismic experiment , Tectonophysics , 316,1-17, 2000.

Hole, J. A., and Zelt, B. C., Three dimension finite difference reflection travel times, Geophys. J. Int., 121, 427-434 , 1995.

Horasan, G., Gülen, L., Pınar, A., Kalafat, D., Özel, N., Kuleli, H.S., Işıkara, A.M., Litospheric Structure of the Marmara and Aegean Regions, Western Turkey, Bulletin of the Seismological Society of America , 92,1, 322-329, 2002.

Hubert-Ferrari, A., Armijo, R., King, G.C.P., Meyer, B., and Barka, A., Morphology, Displacement and Slip Rates Along the North Anatolian Fault (Turkey), J. Geophys. Res., 107, B10, ETG9-1-ETG-33, 2002a.

Imren,C., Pichon,X.Le., Rangin, C., Demirbağ, E., Ecevitoğlu, B., Görür, N., The North Anatolian Fault within the Sea of Marmara :a new interpretation based on multi-channel seismic and multi-beam bathymetry data , Earth and Planetary Science Letters ,186, 143-158, 2001.

Irikura, K., Prediction of Strong Acceleration Motion Using Emprical Green's Function, 7th Japan. Earthq. Eng. Symp. 151-156, 1986.

Jost, M.L., and Herrmann, R.B., A Student's Guide to and Review of Moment Tensors, Seismological Research Letters , 60 , No . 2, 1989.

Kamae, K., Irikura, K., Pitarka, A., A Technique for Simulating Strong Ground Motion Using Hybrid Green's Function, Bulletin of the Seismological Society of America , 88, 2 , 357-367, 1998.

Karabulut, H., Özalaybey, S., Taymaz, T., Aktar, M., Selvi, O., Kocaoğlu, A., A Tomographic İmage of the Shallow Crustal Structure in the Eastern Marmara, Geophysical Research Letters, 30, 24, 2277, 2003.

Karahan, A.E., Berckhemer, H., Baier, B., Crustal structure at the western end of the North Anatolian Fault Zone from deep seismic sounding, Annali Di Geopfisica, 44, ,1, 49-68, 2001.

Ketin, İ., Uber die teknoniscmechanischen Folgerungen Aus Den Grossen Anatolischen Erdbeben Des Letzten Dezenniums, Geol. Rundschau, 36, 77-83, 1948.

McClusky, S., Balassanian S., Barka, A., Demir C., Ergintav, S., Georgiev, I., Gürkan, O., Hamburger, M., Hurst, K., Kahle, H., Kastens K., Kekelidze, K., King, R., Kotzev, V., Lenk, O., Mahmoud, S., Mishin, A., Nadariya, M., Ouzounis, A., Paradissis, D., Peter, Y., Prilepin, M., Reilinger, R., Sanlı, I., Seeger, H., Tealeb, A., Toksöz, M. N., Veis, G., Global Positioning System Constraints on Plate Kinematics and Dynamics in the Eastern Mediterranean and Caucasus, J. Geophys. Res. 105, 5695-5719, 2000.

Nakamura A., Hasegawa, A., Ito, A., Ucer, B., Baris, S., Honkura, Y., Kano, T.,Hori, S., Pektas, R., Komut, T., Çelik, C., Isikara, A., P-wave velocity structure of the crust and its relationship to the Occurrence of the 1999 Izmit, Turkey, Earthquake and Aftershocks, Bulletin of Seismological Society of America, 92, 1, 330-338, 2002.

Okay, A.I., Kaşlılar-Özcan, A., İmren, C., Boztepe-Güney, A., Demirbağ, E., Kuşçu, İ., Active Faults and evolving strike-slip basins in the Marmara Sea, northwest Turkey: a multichannel seismic reflection study , Tectonophysics , 321 , 189-218, 2000.

Orgulu, G., And Aktar, M., Regional Moment Tensor Inversion for Strong Aftershocks of the August 17, 1999 Izmit Earthquake (Mw-7.4), Geophy. Res. Lett., 28,371-374, 2001.

Orgulu, G., Analysis of Regional Moment Tensor Inversion Method and Its Applications to the Izmit, Duzce Earthquake Sequences And Eastren Anatolian Earthquakes, Ph.D. Thesis, Bogazici University, 2002.

Ozalaybey, S., Ergin, M., Aktar, M., Tapırdamaz, C., Biçmen, F., Yörük, A., The 1999 İzmit Erathquake sequences in Turkey: Seismological and Tectonic Aspects, Bull. Seism. Soc. Am.,92, 1.pp, 376-386, 2002.

Parke, J.R. et al., Active Faults in the Sea of Marmara Sea, Western Turkey, Imaged by Seismic Reflection Profiles, Terra Nova, 11, 223-227, 1999.
Pichon, X.Le., Taymaz, T., Şengör, A.M.C., The Marmara Fault and The Future Istanbul Eaerhquake, Proceeding of ITU-IAHS, International Conference On The Kocaeli Earthquake 17 August 1999, Istanbul-Turkey, 2-5 December 1999, pp. 41-54, 1999.

Pichon, X.Le., Şengör, A.M.C., Demirbağ, E., Rangin, C., İmren, C., Armijo, R., Görür, N., Çağatay, N., Mercier de Lepinay, B., Meyer, B., Saatçılar, R., Tok, B., The active Main Marmara Fault , Earth and Planetary Science Letters , 192 , 595-616, 2001.

Pulido, N., Ojeda, A., Atakan, K., Kubo, T., Strong Ground Motion Estimation at Istanbul (Turkey) Based on an Earthquake Scenario: Preliminary Results, Japan Earthquake Engineering Symposium, 2002.

Somerville, P., Irikura, K., Graves, R., Sawada, S., Wald, D., Abrahamson, N., Iwasaki, Y., Kagawa, T., Smith, N., and Kowada, A., Characterizing Crustal Earthquake Slip Models for the Prediction of Strong Ground Motion, Seismological Research Letters, Vol. 70, No. 1, 1999.

Smith, A.D, Taymaz, T. et al., High Resolution Seismic Profiling in the Sea of Marmara (NW Turkey): Late Quaternary Sedimentation and Sea-Level Changes, Bull. Geol. Soc. Am., 107 (8), 923-936, 1995.

Stein, R., et al., Progressive Failure on the North Anatolian Fault since 1939 by Earthquake Stress Triggering, Geophys. J. Int., 128, 594-604, 1997.

Straub, C., Khale, H-G., and Schindler, C., GPS and Geologic Estimates of Tectonic Activity in the Marmara Sea Region, Nw Anatolia, J. Geophys. Res., 102, 27 587-27 601, 1997.

Uçer, B., Eyidogan, H., Gürbüz, C., Barka, A., Şerif B., Seismic İnvestigations of Marmara Region in Active Tectonics of Northwest Anatolia. In: Schindler, C., Pfister, M. (Eds.), The Marmara Poly-Project. Hochschulverlag AG an Der ETH, Zurrich, pp.55-87, 1997.

Taymaz, T., Jackson, J.A., McKenzie, D., Active Tectonics of the North and Central Aegean Sea, Geophys. J. Int., 106, 433-490, 1991.

Vidale, J. E., Finite difference calculation of travel times, Bull. Seism. Soc. Am., 78, 2062-2076 , 1988.

Zor, E., The Shear Wave Velocity Structure of the Eastern Marmara Region by using Receiver Function Analysis, Ph.D. Thesis, Bogazici University, 2002